

Supporting Information

In the Context of Polymorphism: Accurate Measurement and Validation of Solubility Data

Víctor Vázquez Marrero,^{1,2} Carmen Piñero Berríos,^{2,3} Luz De Dios Rodríguez,^{1,2} Torsten Stelzer^{2,4*} and
Vilmali López-Mejías^{2,3*}

¹Department of Biology, University of Puerto Rico - Río Piedras Campus,
San Juan, Puerto Rico, 00931, United States

²Crystallization Design Institute, Molecular Sciences Research Center,
University of Puerto Rico, San Juan, Puerto Rico 00926, United States

³Department of Chemistry, University of Puerto Rico - Río Piedras Campus,
San Juan, Puerto Rico, 00931, United States

⁴Department of Pharmaceutical Sciences, University of Puerto Rico - Medical Sciences Campus,
San Juan, Puerto Rico, 00936, United States

*E-mail: torsten.stelzer@upr.edu (T.S.)

*E-mail: vilmali.lopez@upr.edu (V.L.-M.)

1 Materials

Table S1 shows the CAS number, corresponding source, purity (determined by chemical supplier), analysis method, and solvent classification of the materials employed in this study. All materials were used “as received” without further purification.

Table S1. Sources and percent purity of materials with corresponding analysis method. Solvents are listed with increasing chain length of the homologues series.

Chemical name	CAS registry number	Source	Percentage purity ^a	Purification method	Analysis method	Solvent classification ^b
flufenamic acid	530-78-9	Sigma-Aldrich	≥97%	none	TLC	-
niflumic acid	4394-00-7	Sigma-Aldrich	≥98%	none	TLC	-
tolfenamic acid	13710-19-5	Sigma-Aldrich	≥98%	none	TLC	-
methanol	67-56-1	VWR	99.8%	none	GC	Class 2
ethanol (200-proof)	64-17-5	Pharmco Aaper	≥99.9%	none	GC	Class 3
1-propanol	71-23-8	Alfa-Aesar	99.5%	none	GC	Class 3
<i>n</i> -butanol	71-36-3	Sigma-Aldrich	99.9%	none	FCC, FG	Class 3

^a Provided by the suppliers.

2 Preparation of Metastable Polymorphs

Commercial flufenamic acid (FFA) form I and tolfenamic acid (TA) form I were recrystallized from methanol and ethanol to produce FFA form III² and TA form II,³ respectively. The resulting solids were filtered, vacuum-dried at room temperature, and characterized by Raman microscopy and powder micro X-ray diffraction (PXRD) to determine the phase and purity. When recrystallized from methanol, ethanol, 1-propanol, and *n*-butanol, niflumic acid (NA) yielded the commercial polymorphic form, which is the only known form for this compound.

3 Differential Scanning Calorimetry (DSC)

Samples were analyzed using a DSC Q2000 (TA Instruments Inc.) equipped with a RCS40 single-stage refrigeration system and auto sampler. The calibration of the instrument was made with an indium standard ($T_m = 428.75$ K and $\Delta_{fus}H = 28.54$ J/g). Approximately 2 mg of the powder samples were weighed using a XP26 microbalance from Mettler Toledo (± 0.002 mg) and placed on hermetically sealed aluminum pans. Samples were equilibrated at 298.15 K for 10 min prior to heating to 573.15 K under N₂ atmosphere (50 mL/min) at a rate of 10 K/min and temperature accuracy of 0.1 K. A total of five ($n = 5$) samples were analyzed. Representative thermographs of FFA forms I and III, TA forms I and II, and NA are shown in Figures S1-S5. The area under the curve represents the enthalpy of fusion, in J·g⁻¹. *Universal Analysis software* from TA Instruments Inc. (version 4.5A) was employed for the data analysis and interpretation. To obtain the value for the enthalpy of fusion in kJ·mol⁻¹, the enthalpy of fusion in J·g⁻¹ was multiplied by the molecular mass of FFA, NA and TA (281.230, 261.707, and 282.218 g·mol⁻¹, respectively) and divided by 1,000. The average $\Delta_{fus}H$, and $T_{m,onset}$ (onset melting temperature) obtained are

shown in Tables S2-S6. The average value of $T_{m, \text{onset}}$ was employed to calculate the predicted mole fraction solubility (x_1^{cal}) using the λh model equation.

Table S2. Thermodynamic properties of FFA form I at a pressure (p), p = 101.3 kPa.^a

	$T_{m, \text{onset}}/\text{K}$	$\Delta_{fus}H/\text{kJ}\cdot\text{mol}^{-1}$
	406.67	27.4
	406.67	27.6
	406.68	27.2
	406.64	26.8
	406.67	27.7
Average (n= 5)	406.67	27.3
Standard deviation	0.02	0.4

^aRelative standard uncertainty u is u(p) = 0.1.

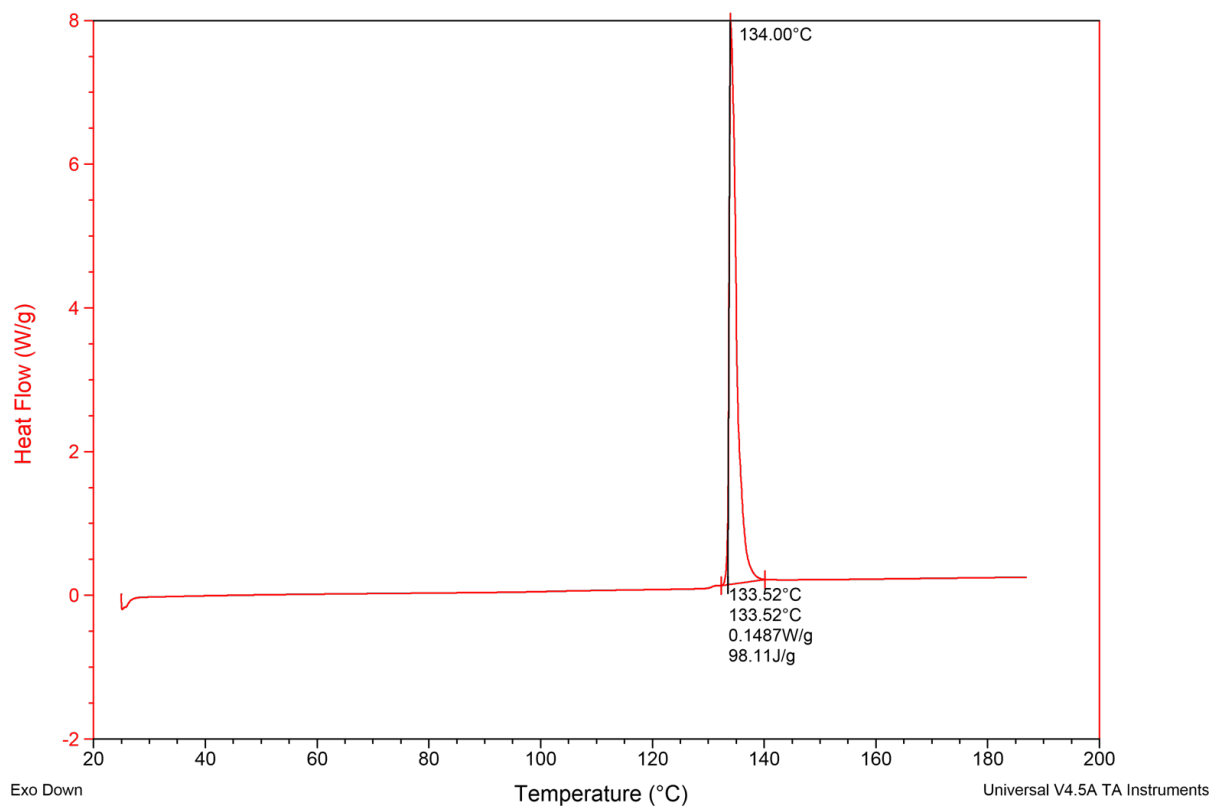


Figure S1. A representative DSC thermogram of FFA form I.

Table S3. Thermodynamic properties of FFA form III at a pressure (p), p = 101.3 kPa.

	$T_{m, onset}/K$	$\Delta_{fus}H/kJ \cdot mol^{-1}$
	399.33	27.1
	399.41	27.1
	399.25	27.9
	399.35	27.6
	399.30	27.9
Average (n= 5)	399.33	27.5
Standard deviation	0.06	0.4

Relative standard uncertainty u is $u(p) = 0.1$.

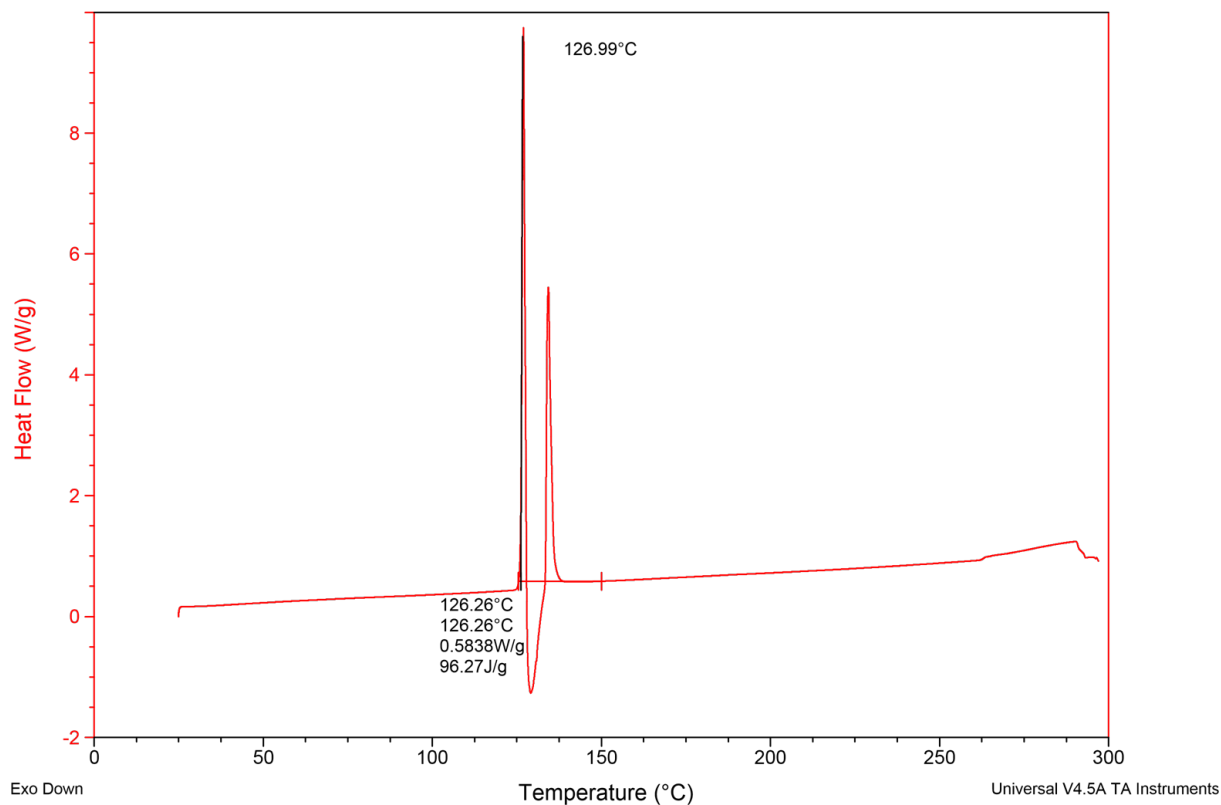


Figure S2. A representative DSC thermogram of FFA form III showing the melting of FFA form III followed by the exothermic recrystallization of FFA form I before its melting.

Table S4. Thermodynamic properties of TA form I at a pressure (p), p = 101.3 kPa.

	$T_{m, onset}/K$	$\Delta_{fus}H/kJ \cdot mol^{-1}$
	485.21	38.5
	485.14	38.4
	485.18	38.2
	485.18	38.1
	485.13	38.8
Average (n= 5)	485.17	38.4
Standard deviation	0.03	0.3

Relative standard uncertainty u is u(p) = 0.1.

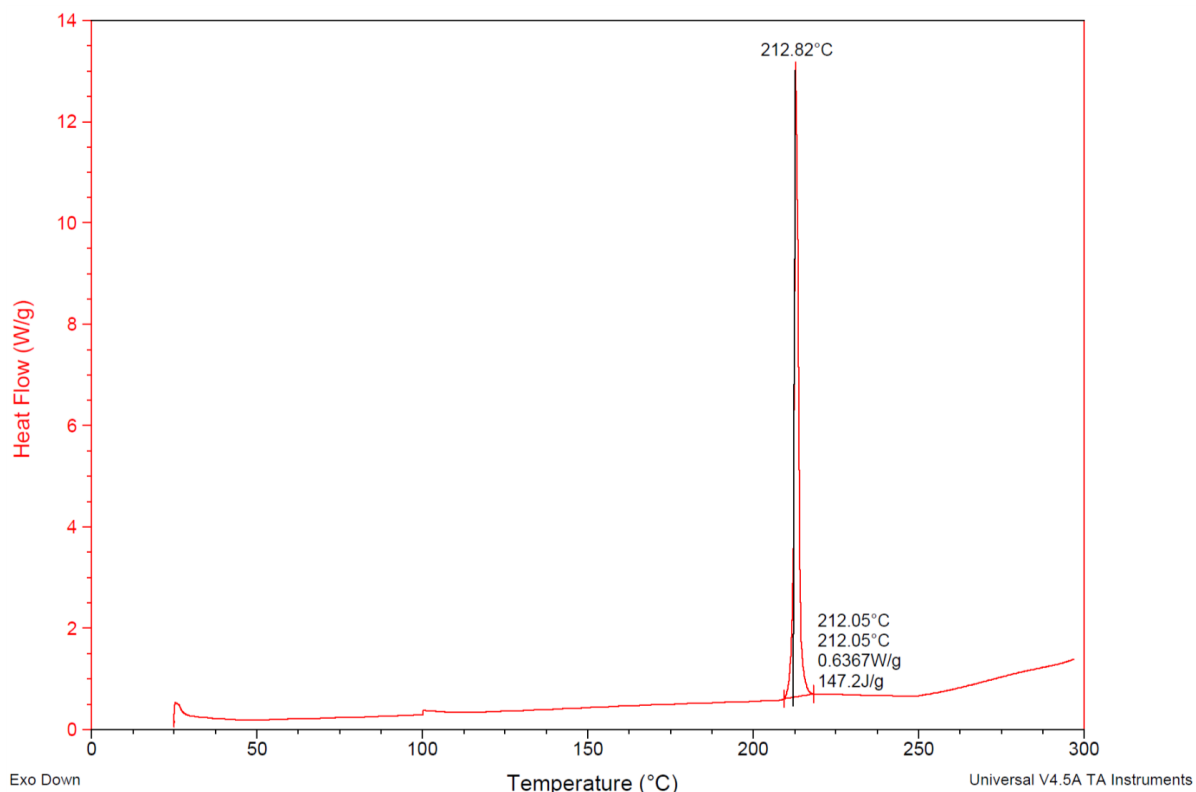


Figure S3. A representative DSC thermogram of TA form I.

Table S5. Thermodynamic properties of TA form II at a pressure (p), p = 101.3 kPa.^a

	$T_{m, onset}/K$	$\Delta_{fus}H/kJ\cdot mol^{-1}$
	485.4	39.4
	485.6	39.1
	485.4	39.2
	485.5	39.0
	485.9	38.8
Average (n= 5)	485.6	39.1
Standard deviation	0.2	0.2

^aRelativ standard uncertainty u is u(p) = 0.1.

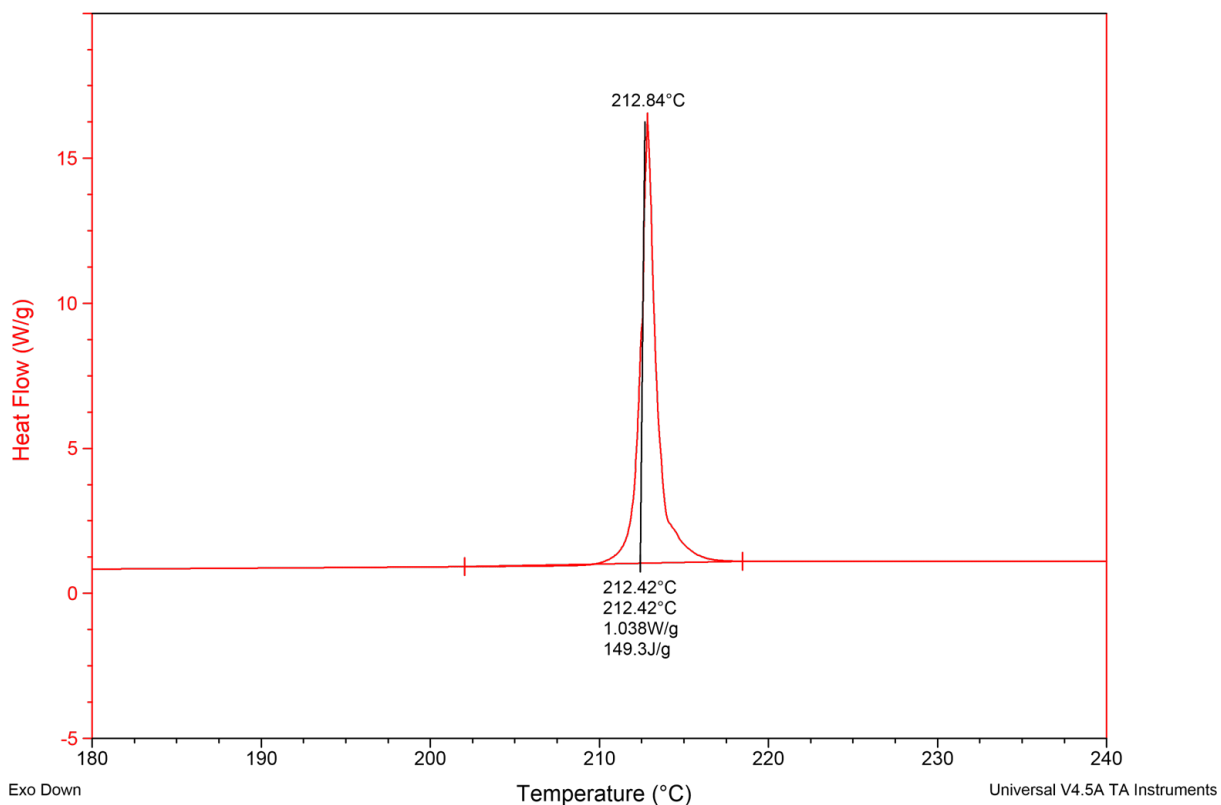


Figure S4. A representative DSC thermogram of TA form II.

Table S6. Thermodynamic properties of NA at a pressure (p), p = 101.3 kPa.

	$T_{m, \text{onset}}/K$	$\Delta_{fus}H/kJ \cdot mol^{-1}$
	475.53	34.7
	475.49	34.2
	475.50	35.2
	475.61	35.9
	475.54	34.4
Average (n= 5)	475.53	34.9
Standard deviation	0.05	0.7

Relative standard uncertainty u is u(p) = 0.1.

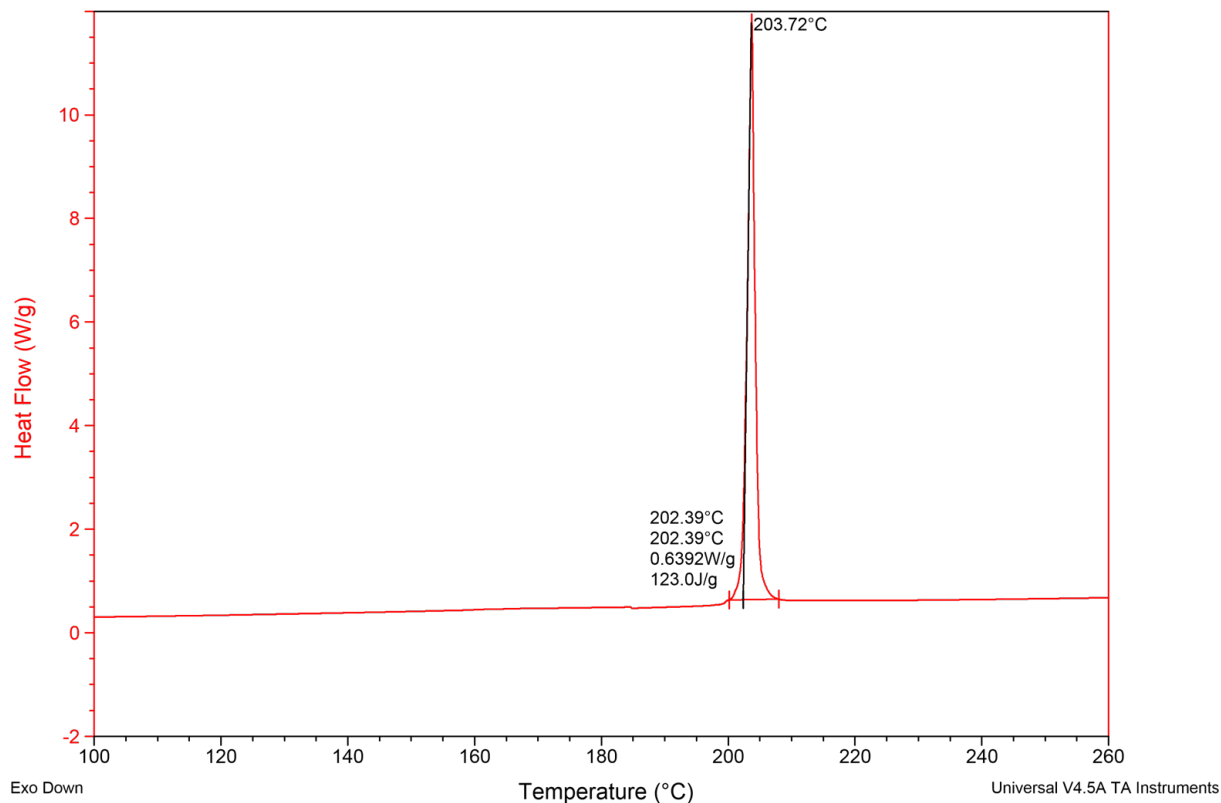


Figure S5. A representative DSC thermogram of NA.

To confirm the accuracy of the onset melting temperatures ($T_{m, \text{onset}}$) obtained for the selected compounds and polymorphs thereof within this work, the $T_{m, \text{onset}}$ was compared to peak melting temperatures ($T_{m, \text{peak}}$) reported in literature (Table S7).

Table S7. Comparison of the onset melting temperature ($T_{m, \text{onset}}$) for the selected compounds and polymorph thereof with peak melting temperatures ($T_{m, \text{peak}}$) reported in literature. If the standard deviation for T_m is not listed it was not provided in the reference cited.

Compound	Polymorph	T_m /K	References
FFA	I	406.67 ± 0.02	This work ^a
	I	407.15	4
	I	407.1	5
	I	407.65	6
	III	399.33 ± 0.06	This work ^a
	III	400.55	6
	III	398.1	5
TA	I	485.17 ± 0.03	This work ^a
	I	486.25	7
	I	484.05	3
	II	485.6 ± 0.2	This work ^a
	II	487.65	3
NA		475.53 ± 0.05	This work ^a
		476.80	8
		476.3	5

^aThe onset melting temperatures, $T_{m, \text{onset}}$, was used in this work.

The peak melting temperatures ($T_{m, \text{peak}}$) reported in the literature for FFA forms I and III has an average of 407.3 ± 0.3 K and 399 ± 2 K, respectively. Here, we report and use the $T_{m, \text{onset}}$ (406.67 ± 0.02 K and 399.33 ± 0.06 K, respectively) and find these are in close agreement with the published data for these polymorphs. For the TA polymorphs, the $T_{m, \text{peak}}$ reported in the literature for forms I and II corresponds to 485 ± 2 K and 487.2 ± 0.7 K, respectively. The $T_{m, \text{onset}}$ determined in this work (485.17 ± 0.03 K and 485.6 ± 0.2 K, respectively) are in close agreement with that of the published data for both polymorphs. Lastly, the $T_{m, \text{peak}}$ reported in the literature for NA is 476.5 ± 0.4 K, thus the $T_{m, \text{onset}}$ determined in this work (475.53 ± 0.05 K) is in close agreement with that of the published data.

4 Solubility Measurement

The polythermal method was used in an attempt to determine the solubility of FFA (forms I and III), TA (forms I and II), and NA in methanol, ethanol, 1-propanol, *n*-butanol using a Crystal16™ multiple reactor system (Technobis Crystallization Systems).⁹⁻¹⁶ Samples with different concentrations were prepared in sealed glass vials (Fisher Scientific) with an internal volume of 2 mL using a XP26 microbalance from Mettler Toledo (± 0.002 mg) to weigh the solute and a MS104S analytical balance from Mettler Toledo (± 0.1 mg) to weigh the pure solvents. The resulting suspensions were agitated using a magnetic stir bar (rare earth) at 700 rpm while heated from 278.15 to 333.15 K at 0.3 K/min.¹⁶ For FFA form I, a temperature range between 318.15 and 333.15 K was employed, as this form is metastable below 315.15 K (transition temperature 42 °C).¹⁷ Any measurement attempts below 315.15 K, resulted in a solvent-mediated phase transformation to FFA form III. On this account, at the end of the temperature cycles, the temperature was kept at 318.15 K to avoid transformation to FFA form III. Assuming that

dissolution kinetics can be neglected,¹³ monitoring the transmission of light through the suspension can be used to determine the saturation temperature at its maximum^{11-15,18} using the software CrystalClear (v 1.0.1.614). To ensure accuracy, the saturation temperature at a specific concentration was measured at least twice. The uncertainty of each saturated temperature measurement was within ± 0.1 K. Figures S6-S8 present the experimentally measured and correlated solubility data using the λh model equation for FFA forms I and III, TA form I, and NA in each pure solvent employed in this investigation (values are shown in Tables S8-S11).

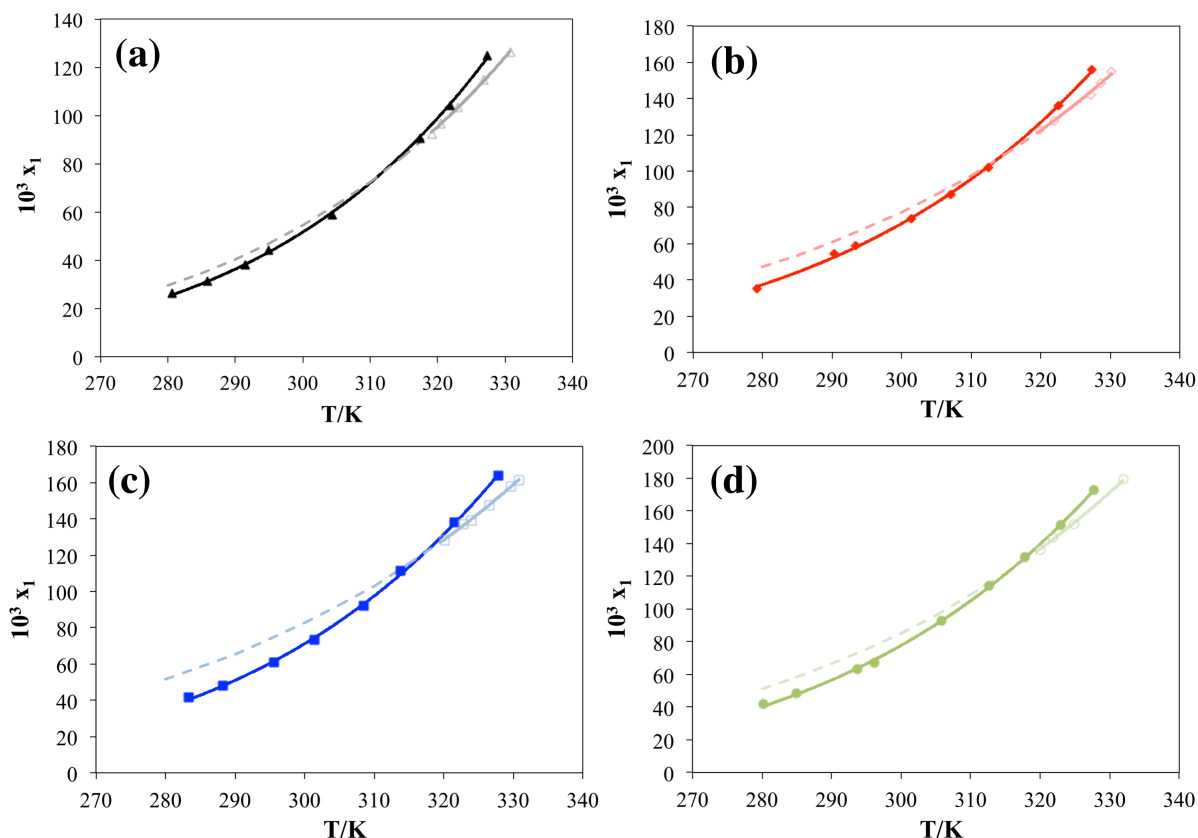


Figure S6. Experimental and correlated solubility data of FFA forms I and III in (a) methanol, (b) ethanol, (c) 1-propanol, and (d) *n*-butanol. Open symbols, Δ , \diamond , \square , and \circ , represent experimental data points for FFA form I; and filled symbols, \blacktriangle , \blacklozenge , \blacksquare , and \bullet , represent experimental data points for FFA form III, the trend lines were calculated using λh equation, solid dark and brighter lines represent FFA forms I and III, respectively. Dashed lines represent the extrapolation of the solubility data for FFA form I.

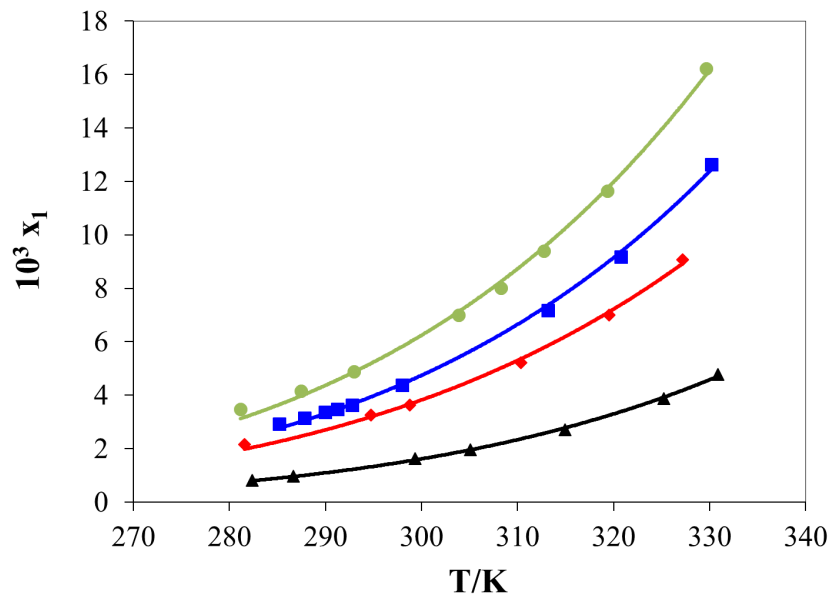


Figure S7. Experimental and correlated solubility data of TA form I in four alcohols of a homologous series. \blacktriangle , methanol; \blacklozenge , ethanol; \blacksquare , 1-propanol; \bullet , *n*-butanol; the solid trend lines were calculated using λh equation.

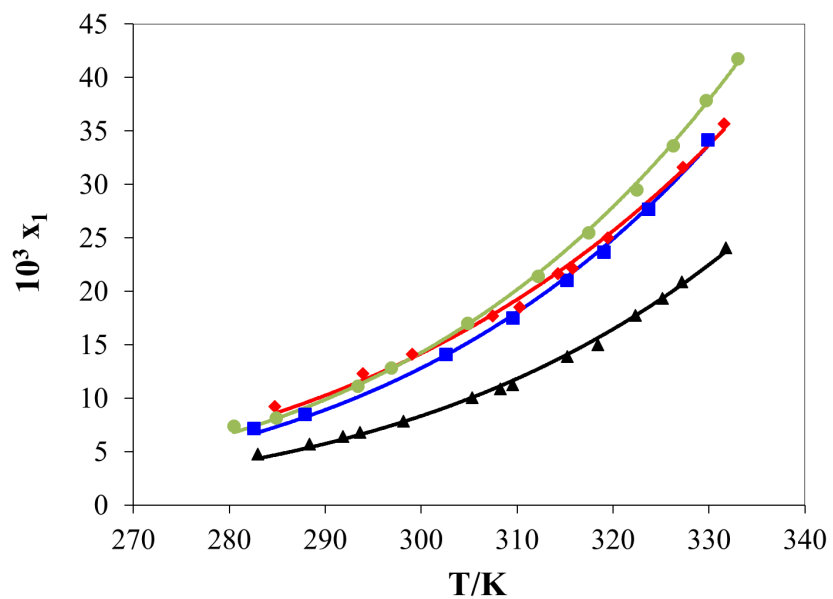


Figure S8. Experimental and correlated solubility data of NA in four alcohols of a homologous series. \blacktriangle , methanol; \blacksquare , 1-propanol; \blacklozenge , ethanol; \bullet , *n*-butanol; the solid trend lines were calculated using λh equation.

Table S8. Experimental and correlated mole fraction solubility of FFA form III in methanol, ethanol, 1-propanol, and *n*-butanol at different temperatures T and at pressure $p = 101.3 \text{ kPa}^{b,d}$

T/K	$10^3 x_1^{exp}$	Apelblat		λh		T/K	$10^3 x_1^{exp}$	Apelblat		λh	
		$10^3 x_1^{cal}$	10 ³ RD	$10^3 x_1^{cal}$	10 ³ RD			$10^3 x_1^{cal}$	10 ³ RD	$10^3 x_1^{cal}$	10 ³ RD
Methanol						Ethanol					
280.7	26.36	26.44	-0.30	25.65	2.70	279.2	35.23	36.76	-4.37	36.29	-3.04
285.9	31.34	31.65	-0.97	31.21	0.43	290.4	54.28	52.68	2.95	52.60	3.08
291.5	37.96	38.33	-0.96	38.28	-0.85	293.5	58.83	58.03	1.37	58.05	1.34
295.0	44.30	43.16	2.60	43.35	2.15	301.4	73.89	73.85	0.05	74.05	-0.22
304.4	58.72	59.11	-0.67	59.82	-1.87	307.1	86.97	87.47	-0.58	87.74	-0.88
317.4	90.66	90.47	0.20	91.09	-0.47	312.6	101.93	102.65	-0.70	102.89	-0.93
321.9	104.17	104.57	-0.39	104.76	-0.57	322.6	136.05	136.16	-0.08	136.13	-0.06
327.4	124.81	124.60	0.16	123.86	0.76	327.4	155.73	155.37	0.23	155.11	0.40
1-propanol						n-butanol					
283.4	41.73	40.52	2.90	40.35	3.31	280.3	42.02	41.18	2.01	40.64	3.28
288.3	48.03	48.07	-0.08	47.98	0.11	285.0	48.58	48.10	0.98	47.77	1.67
295.7	60.82	61.69	-1.43	61.70	-1.46	293.8	63.11	63.81	-1.11	63.84	-1.16
301.4	73.29	74.26	-1.33	74.34	-1.43	296.2	67.20	68.79	-2.37	68.92	-2.56
308.5	91.88	92.86	-1.07	92.97	-1.19	305.9	92.59	92.51	0.09	92.89	-0.32
313.9	111.22	109.49	1.56	109.58	1.47	312.7	114.11	113.08	0.90	113.45	0.58
321.6	138.20	137.43	0.55	137.44	0.55	317.9	131.85	131.35	0.37	131.59	0.19
327.9	163.75	164.51	-0.46	164.41	-0.40	323.0	151.40	151.70	-0.19	151.66	-0.17
						327.8	172.99	173.27	-0.16	172.81	0.10

Standard uncertainty u is $u(T) = 1 \text{ K}$. Relative standard uncertainties u are $u(p) = 0.1$, $u(x_i) = 0.01$. x_1^{exp} refers to the experimental mole fraction solubility. x_1^{cal} refers to the calculated solubility data using Apelblat and λh model equations. RD represents the corresponding relative deviation.

Table S9. Experimental and correlated mole fraction solubility of FFA form I in methanol, ethanol, 1-propanol, and *n*-butanol at different temperatures T and at pressure $p = 101.3 \text{ kPa}^{b,d}$

T/K	$10^3 x_1^{exp}$	Apelblat		λh		T/K	$10^3 x_1^{exp}$	Apelblat		λh	
		$10^3 x_1^{cal}$	10 ³ RD	$10^3 x_1^{cal}$	10 ³ RD			$10^3 x_1^{cal}$	10 ³ RD	$10^3 x_1^{cal}$	10 ³ RD
Methanol						Ethanol					
319.2	92.51	93.13	-0.67	93.13	-0.67	319.9	122.78	122.05	0.60	122.09	0.56
320.5	96.82	96.44	0.38	96.44	0.39	322.0	127.85	127.96	-0.09	127.96	-0.09
323.1	103.56	103.39	0.16	103.39	0.17	327.3	142.13	144.00	-1.32	143.96	-1.29
326.9	114.74	114.34	0.34	114.34	0.35	328.7	148.43	148.51	-0.05	148.49	-0.04
330.8	126.31	126.63	-0.25	126.65	-0.26	330.3	155.16	153.82	0.86	153.83	0.85
1-propanol						n-butanol					
320.2	128.37	128.67	-0.23	128.72	-0.27	319.95	136.30	136.61	-0.23	136.64	-0.25
322.9	137.10	136.42	0.50	136.41	0.51	321.85	143.89	142.67	0.85	142.67	0.85
324.0	139.30	139.69	-0.28	139.66	-0.26	324.95	151.86	153.05	-0.78	153.02	-0.76
326.6	147.72	147.69	0.02	147.65	0.05	331.95	179.18	178.91	0.15	178.91	0.15
329.7	157.92	157.74	0.11	157.74	0.11						
330.9	161.59	161.79	-0.12	161.83	-0.14						

Standard uncertainty u is $u(T) = 1 \text{ K}$. Relative standard uncertainties u are $u(p) = 0.1$, $u(x_i) = 0.01$. x_1^{exp} refers to the experimental mole fraction solubility. x_1^{cal} refers to the calculated solubility data using Apelblat and λh model equations. RD represents the corresponding relative deviation.

Table S10. Experimental and correlated mole fraction solubility of TA form I in methanol, ethanol, 1-propanol, and *n*-butanol at different temperatures T and at pressure $p = 101.3 \text{ kPa}^{b,c,d}$

T/K	$10^4 x_1^{exp}$	Apelblat		λh		T/K	$10^4 x_1^{exp}$	Apelblat		λh	
		$10^4 x_1^{cal}$	10% RD	$10^4 x_1^{cal}$	10% RD			$10^4 x_1^{cal}$	10% RD	$10^4 x_1^{cal}$	10% RD
Methanol						Ethanol					
282.4	0.82	0.85	-3.43	0.80	2.41	281.6	2.15	2.18	-1.65	1.98	7.74
286.7	0.97	0.99	-1.73	0.96	1.92	294.8	3.25	3.21	1.37	3.20	1.77
299.4	1.63	1.57	3.34	1.58	2.91	298.8	3.64	3.62	0.44	3.67	-0.70
305.1	1.96	1.93	1.46	1.95	0.16	310.4	5.21	5.22	-0.16	5.36	-2.94
315.0	2.70	2.73	-1.24	2.78	-2.83	319.6	6.99	7.03	-0.54	7.12	-1.86
325.3	3.88	3.91	-0.90	3.93	-1.30	327.2	9.07	9.05	0.23	8.92	1.65
330.9	4.77	4.74	0.57	4.71	1.32						
1-propanol						<i>n</i>-butanol					
285.2	2.93	2.90	1.27	2.76	5.92	281.2	3.48	3.42	1.71	3.12	10.25
287.8	3.15	3.15	-0.01	3.05	3.04	287.5	4.17	4.16	0.12	3.98	4.60
290.0	3.38	3.37	0.26	3.31	2.09	293.0	4.88	4.95	-1.52	4.87	0.16
291.3	3.47	3.51	-1.09	3.47	0.09	303.9	7.00	7.01	-0.08	7.12	-1.70
292.8	3.64	3.68	-1.16	3.66	-0.70	308.3	8.02	8.08	-0.72	8.25	-2.83
298.0	4.37	4.35	0.54	4.42	-0.96	312.8	9.40	9.35	0.53	9.55	-1.56
313.2	7.18	7.15	0.46	7.37	-2.56	319.4	11.64	11.59	0.42	11.75	-0.91
320.8	9.18	9.21	-0.29	9.37	-2.02	329.7	16.23	16.25	-0.15	16.01	1.33
330.2	12.63	12.62	0.04	12.44	1.50						

Standard uncertainty u is $u(T) = 1 \text{ K}$. Relative standard uncertainties u are $u(p) = 0.1$, $u(x_1) = 0.01$. x_1^{exp} refers to the experimental mole fraction solubility. x_1^{cal} refers to the calculated solubility data using Apelblat and λh model equations. RD represents the corresponding relative deviation.

Table S11. Experimental and correlated mole fraction solubility (x_1) of NA in methanol, ethanol, 1-propanol, and *n*-butanol at different temperatures T and at pressure $p = 101.3 \text{ kPa}^{b,c,d}$

T/K	$10^4 x_1^{exp}$	Apelblat		λh		T/K	$10^4 x_1^{exp}$	Apelblat		λh	
		$10^4 x_1^{cal}$	10% RD	$10^4 x_1^{cal}$	10% RD			$10^4 x_1^{cal}$	10% RD	$10^4 x_1^{cal}$	10% RD
Methanol						Ethanol					
283.0	4.77	4.82	-1.02	4.34	8.89	284.8	9.21	9.41	-2.20	8.58	6.81
288.4	5.69	5.71	-0.37	5.38	5.39	294.0	12.28	12.05	1.89	11.69	4.85
291.9	6.44	6.39	0.82	6.16	4.34	299.1	14.09	13.87	1.53	13.76	2.31
293.6	6.80	6.76	0.66	6.58	3.22	307.5	17.68	17.59	0.54	17.83	-0.82
298.2	7.86	7.83	0.41	7.79	0.90	310.3	18.51	19.06	-2.98	19.38	-4.70
305.3	10.03	9.90	1.24	10.06	-0.33	314.3	21.66	21.40	1.19	21.78	-0.58
308.3	10.87	10.92	-0.52	11.14	-2.55	315.8	22.15	22.36	-0.93	22.74	-2.68
309.6	11.27	11.41	-1.21	11.65	-3.37	319.5	25.01	24.92	0.38	25.26	-1.00
315.3	13.90	13.81	0.66	14.10	-1.46	327.3	31.59	31.45	0.46	31.36	0.74
318.4	14.99	15.35	-2.36	15.62	-4.19	331.6	35.69	35.77	-0.23	35.18	1.44
322.4	17.74	17.56	1.03	17.74	0.01						
325.2	19.31	19.31	0.00	19.37	-0.30						
327.2	20.90	20.68	1.07	20.61	1.40						
331.8	24.07	24.21	-0.56	23.72	1.48						
1-propanol						<i>n</i>-butanol					
282.6	7.19	7.22	-0.42	6.68	7.17	280.5	7.41	7.24	2.38	6.78	8.54
287.9	8.48	8.58	-1.22	8.21	3.21	284.9	8.18	8.44	-3.14	8.08	1.26
302.6	14.10	13.89	1.52	14.02	0.59	293.4	11.16	11.33	-1.54	11.20	-0.29
309.6	17.53	17.48	0.32	17.78	-1.39	296.9	12.84	12.78	0.45	12.74	0.77
315.2	21.06	21.01	0.23	21.35	-1.36	304.9	17.03	16.75	1.65	16.92	0.63
319.1	23.70	23.89	-0.81	24.17	-1.97	312.2	21.44	21.35	0.43	21.66	-1.02
323.7	27.68	27.79	-0.40	27.87	-0.67	317.5	25.48	25.41	0.28	25.74	-1.02
329.9	34.18	34.07	0.32	33.58	1.76	322.5	29.53	29.88	-1.20	30.14	-2.06
						326.3	33.63	33.77	-0.40	33.87	-0.71
						329.7	37.86	37.64	0.59	37.53	0.88
						333.0	41.80	41.79	0.02	41.37	1.02

Standard uncertainty u is $u(T) = 1 \text{ K}$. Relative standard uncertainties u are $u(p) = 0.1$, $u(x_1) = 0.01$. x_1^{exp} refers to the experimental mole fraction solubility. x_1^{cal} refers to the calculated solubility data using Apelblat and λh model equations. RD represents the corresponding relative deviation.

5 Validation of the Heating Rate Employed in the Polythermal Method.

The solubility of FFA forms I and III, TA form I, and NA were determined at 0.3, 0.1 and in case of FFA form III also at 0.05 K/min in the temperature range from 278.15 to 333.15 K in 1-propanol to validate the heating rate employed in the polythermal method (Figures S9-S11). Due to its metastability below 315.15 K,¹⁷ FFA form I was measured in the temperature range from 318.15 K to 333.15 K. Since the solubility of these compounds and polymorphs thereof are not available in the literature, it was decided to employ the solubility measurement at 0.1 K/min as reference to calculate the RD of the experimentally determined saturation temperature for the higher heating rate with respect to the 0.1 K/min ($RD_{0.1\text{ K/min}} = 0$). In case of FFA form III the heating rate of 0.05 K/min was used as reference ($RD_{0.05\text{ K/min}} = 0$). The analysis of these results (Tables S12-S15) showed that the average RD (to maintain positive or negative compared to ARD%) negligibly deviated around the null value from the reference heating rate of 0.1 K/min (for FFA form III 0.05 K/min) when employing 0.3 K/min (and 0.1 K/min for FFA form III) as heating rates. Consequently, a heating rate of 0.3 K/min was employed for further experiments since it provides both accuracy and a fast measurement.^{16,19}

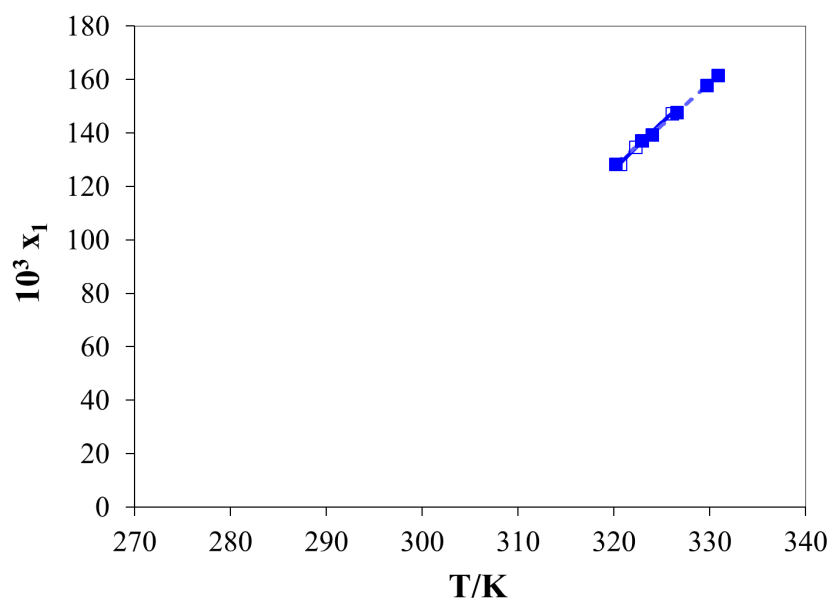


Figure S9. Experimental and correlated solubility data of FFA form I in 1-propanol at different heating rates. □, 0.1 K/min; ■, 0.3 K/min; —, calculated using Apelbat equation.

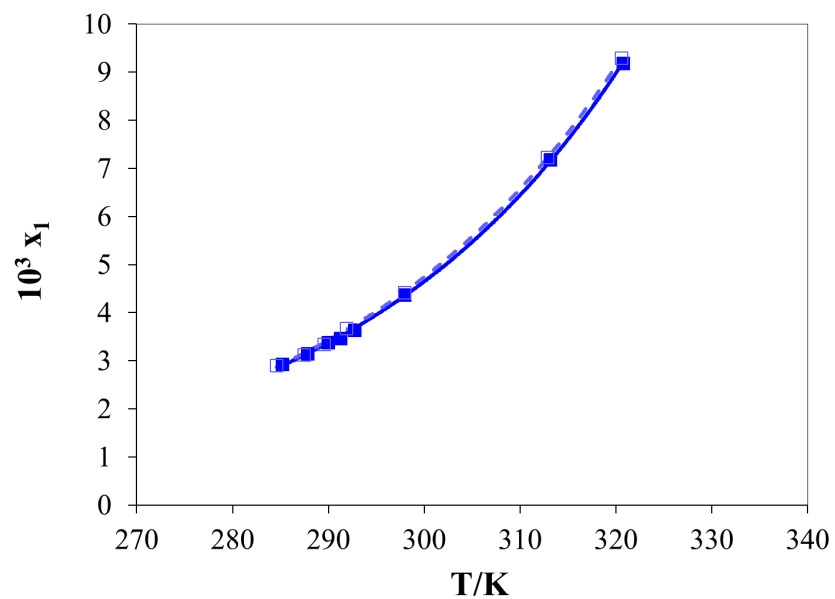


Figure S10. Experimental and correlated solubility data of TA form I in 1-propanol at different heating rates. □, 0.1 K/min; ■, 0.3 K/min; –, calculated using Apelbat equation.

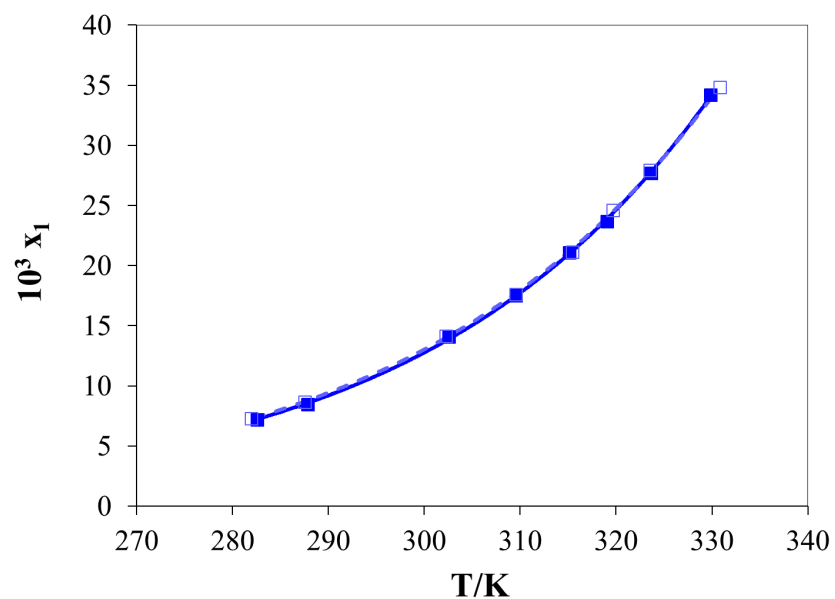


Figure S11. Experimental and correlated solubility data of NA in 1-propanol at different heating rates. □, 0.1 K/min; ■, 0.3 K/min; –, calculated using Apelbat equation.

Table S12. Solubility of FFA form I (x_1) in 1-propanol at different temperatures T (pressure, $p = 101.3$ kPa) measured at a heating rate of 0.1 K/min and compared to a faster heating rate of 0.3 K/min using RD.^a

T/K	$10^3 x_1^{exp}$	$10^3 RD_{0.3}$
320.7	128.38	-0.156
323.0	137.15	-0.031
326.1	147.27	0.153
Average $10^3 RD$		-0.011

^aStandard uncertainty u is $u(T) = 1$ K. Relative standard uncertainties u are $u(p) = 0.1$, $u(x_1) = 0.01$. x_1^{exp} refers to the experimental mole fraction solubility of 1-propanol measured at a heating rate of 0.1 K/min. $RD_{0.3}$ represents the corresponding relative deviation of the determined saturation temperature with the heating rate of 0.3 K/min using the polythermal method.

Table S13. Solubility of FFA form III (x_1) in 1-propanol at different temperatures T (pressure, $p = 101.3$ kPa) measured at a heating rate of 0.05 K/min and compared to faster heating rates of 0.1 K/min and 0.3 K/min using RD.^a

T/K	$10^3 x_1^{exp}$	$10^3 RD_{0.1}$	$10^3 RD_{0.3}$
282.9	42.22	0.071	0.176
288.0	48.80	-0.209	0.104
295.1	61.09	0.000	0.203
308.0	91.04	0.000	0.162
314.3	110.71	-0.032	-0.127
322.2	138.15	-0.093	-0.187
328.2	163.57	0.000	-0.092
Average $10^3 RD$		-0.038	0.034

^aStandard uncertainty u is $u(T) = 1$ K. Relative standard uncertainties u are $u(p) = 0.1$, $u(x_1) = 0.01$. x_1^{exp} refers to the experimental mole fraction solubility of 1-propanol measured at a heating rate of 0.05 K/min. $RD_{0.1}$ and $RD_{0.3}$ represent the corresponding relative deviation of the determined saturation temperature with the heating rate of 0.1 K/min and 0.3 K/min, respectively, using the polythermal method.

Table S14. Solubility of TA form I (x_1) in 1-propanol at different temperatures T (pressure, $p = 101.3$ kPa) measured at a heating rate of 0.1 K/min and compared to a faster heating rate of 0.3 K/min using RD.^a

T/K	$10^3 x_1^{exp}$	$10^3 RD_{0.3}$
284.6	2.90	0.210
287.5	3.13	0.122
289.6	3.35	0.138
291.9	3.67	0.307
298.0	4.42	0.000
312.9	7.23	0.096
320.6	9.29	0.062
Average $10^3 RD$		0.134

^aStandard uncertainty u is $u(T) = 1$ K. Relative standard uncertainties u are $u(p) = 0.1$, $u(x_1) = 0.01$. x_1^{exp} refers to the experimental mole fraction solubility of 1-propanol measured at a heating rate of 0.1 K/min. $RD_{0.3}$ represents the corresponding relative deviation of the determined saturation temperature with the heating rate of 0.3 K/min using the polythermal method.

Table S15. Solubility of NA (x_1) in 1-propanol at different temperatures T (pressure, $p = 101.3$ kPa) measured at a heating rate of 0.1 K/min and compared to a faster heating rate of 0.3 K/min using RD.^a

T/K	$10^3 x_1^{exp}$	$10^3 RD_{0.3}$
282.0	7.31	0.212
287.6	8.67	0.104
302.3	14.14	0.099
309.6	17.62	0.000
315.5	21.15	-0.095
319.7	24.61	-0.188
323.6	27.92	0.031
330.9	34.84	-0.303
Average $10^3 RD$		-0.017

^aStandard uncertainty u is $u(T) = 1$ K. Relative standard uncertainties u are $u(p) = 0.1$, $u(x_1) = 0.01$. x_1^{exp} refers to the experimental mole fraction solubility of 1-propanol measured at a heating rate of 0.1 K/min. $RD_{0.3}$ represents the corresponding relative deviation of the determined saturation temperature with the heating rate of 0.3 K/min using the polythermal method.

6 Raman Spectroscopy

Raman spectra were recorded at room temperature in a Thermo Scientific DXR Raman microscope, equipped with 532 nm laser, 400 lines/nm grating, and 25 μm pinhole. The spectra were collected over the range of 650-1,600 cm^{-1} by averaging 15 scans with 3 s exposures using the software *OMNIC for Dispersive Raman* (version 9.2.0). The commercial powders of FFA form I, TA form I, and NA, as well as the recrystallized FFA form III and TA form II were analyzed by Raman microscopy, and the solid-state were confirmed prior to the solubility measurements.^{6,7} All suspensions were measured by Raman microscopy after the experiments were completed. If Raman spectra for specific concentrations (especially lower concentrations) and compound-solvent systems (especially at lower heating rates of 0.1 and 0.05 K/min) are not shown, no crystalline material could be recovered (samples did not recrystallize in the given experimental time). Figures S12-S23 show Raman spectra of the recovered material at the end of heating/cooling cycle(s) for the data point employed in the solubility curve of each of the compounds and polymorph thereof. We have chosen to include these points in the solubility curve based on the *in situ* and offline solid state characterization. However, we would like to clarify that the recovered crystals at the end of the heating/cooling cycle(s) does not necessarily correspond to that of the starting form employed for each compound and polymorph thereof emphasizing the importance of solid-state monitoring for accurate solubility measurement. In particular, experiments with FFA form I resulted in the recrystallization of FFA form III for all solvents except for methanol (FFA form I).

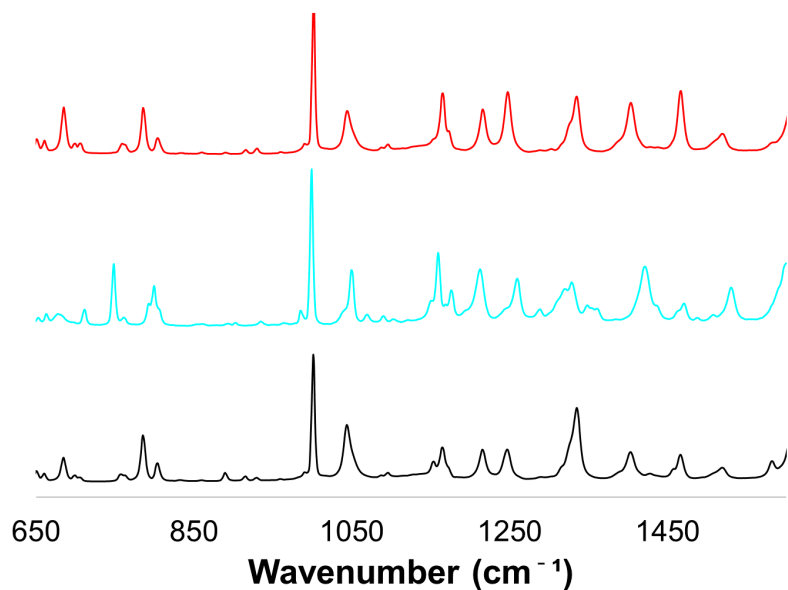


Figure S12. Representative Raman spectra of FFA form I crystals obtained in methanol at a heating rate of 0.3 K/min; $x_1 = 0.1263$ (red), FFA form I (black), and FFA form III (cyan). The other molar fractions ($x_1 = 0.0925$, $x_1 = 0.0968$, $x_1 = 0.1036$, $x_1 = 0.1147$) did not recrystallize; therefore, they were not analyzed.

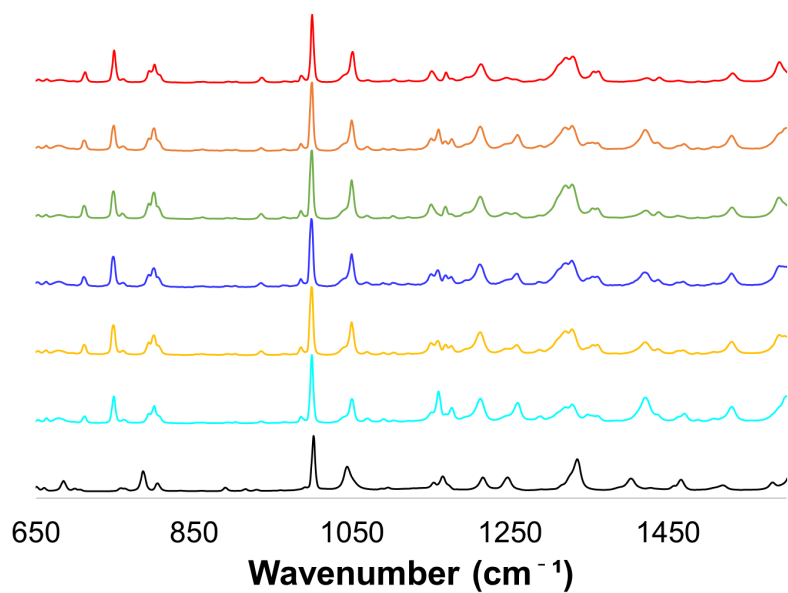


Figure S13. Representative Raman spectra of FFA form III crystals obtained in methanol at a heating rate of 0.3 K/min; $x_1 = 0.1248$ (red), $x_1 = 0.1042$ (orange), $x_1 = 0.0907$ (green), $x_1 = 0.0587$ (blue), $x_1 = 0.0443$ (yellow), FFA form I (black), and FFA form III (cyan). The other molar fractions ($x_1 = 0.0264$, $x_1 = 0.0313$, $x_1 = 0.0380$) did not recrystallize; therefore, they were not analyzed.

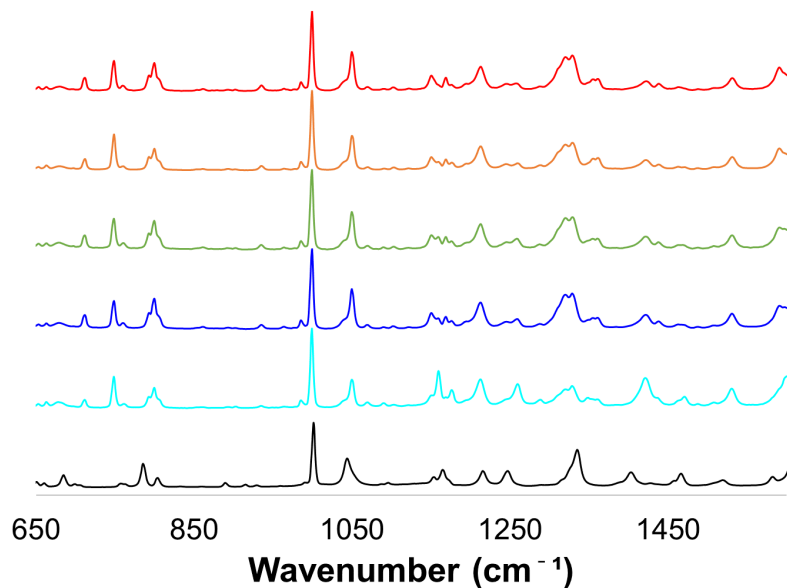


Figure S14. Representative Raman spectra of FFA form I crystals obtained in ethanol at a heating rate of 0.3 K/min; $x_1 = 0.1552$ (red), $x_1 = 0.1493$ (orange), $x_1 = 0.1476$ (green), $x_1 = 0.1421$ (blue), FFA form I (black), and FFA form III (cyan). The other molar fractions ($x_1 = 0.1228$, $x_1 = 0.1278$) did not recrystallize; therefore, they were not analyzed.

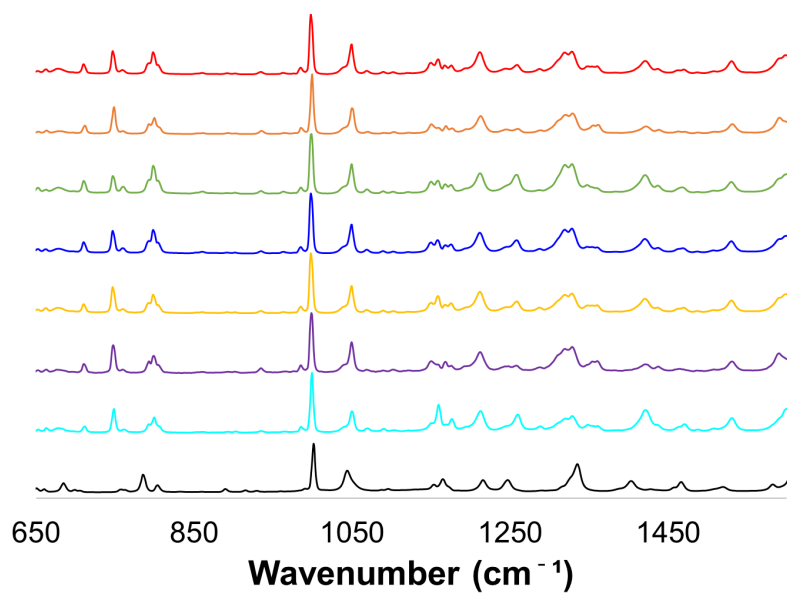


Figure S15. Representative Raman spectra of FFA form III crystals obtained in ethanol at a heating rate of 0.3 K/min; $x_1 = 0.1557$ (red), $x_1 = 0.1493$ (orange), $x_1 = 0.1360$ (green), $x_1 = 0.1019$ (blue), $x_1 = 0.0870$ (yellow), $x_1 = 0.0739$ (purple), FFA form I (black), and FFA form III (cyan). The other molar fractions ($x_1 = 0.0352$, $x_1 = 0.0543$, $x_1 = 0.0588$) did not recrystallize; therefore, they were not analyzed.

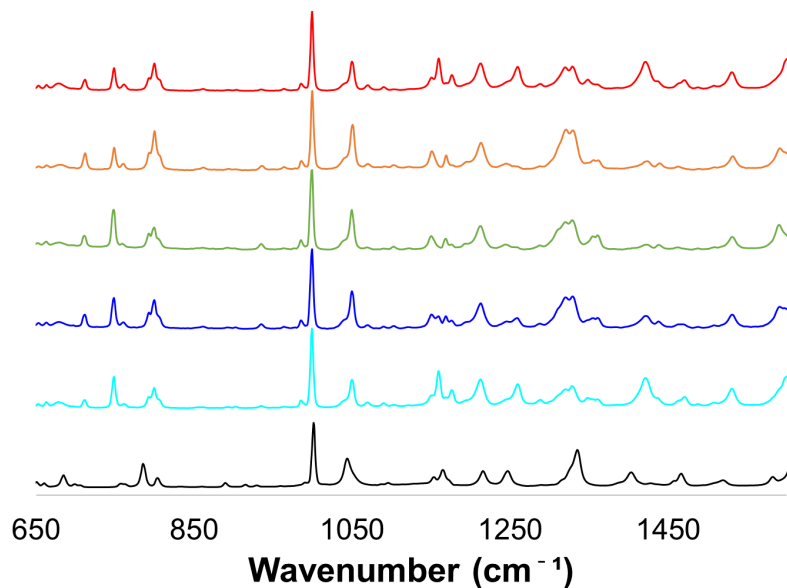


Figure S16. Representative Raman spectra of FFA form I crystals obtained in 1-propanol at a heating rate of 0.3 K/min; $x_1 = 0.1616$ (red), $x_1 = 0.1579$ (orange), $x_1 = 0.1477$ (green), $x_1 = 0.1393$ (blue), FFA form I (black), and FFA form III (cyan). The other molar fractions ($x_1 = 0.1284$, $x_1 = 0.1371$) did not recrystallize; therefore, they were not analyzed.

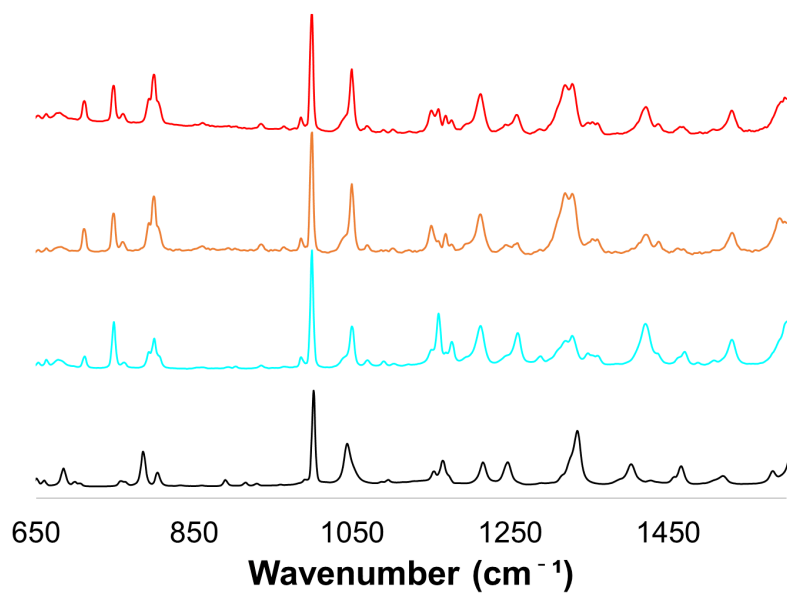


Figure S17. Representative Raman spectra of FFA form I crystals obtained in 1-propanol at a heating rate of 0.1 K/min; $x = 0.1473$ (red), $x = 0.1371$ (orange), FFA form I (black), and FFA form III (cyan). The other molar fractions ($x = 0.1284$, $x = 0.1346$) did not recrystallize; therefore, they were not analyzed.

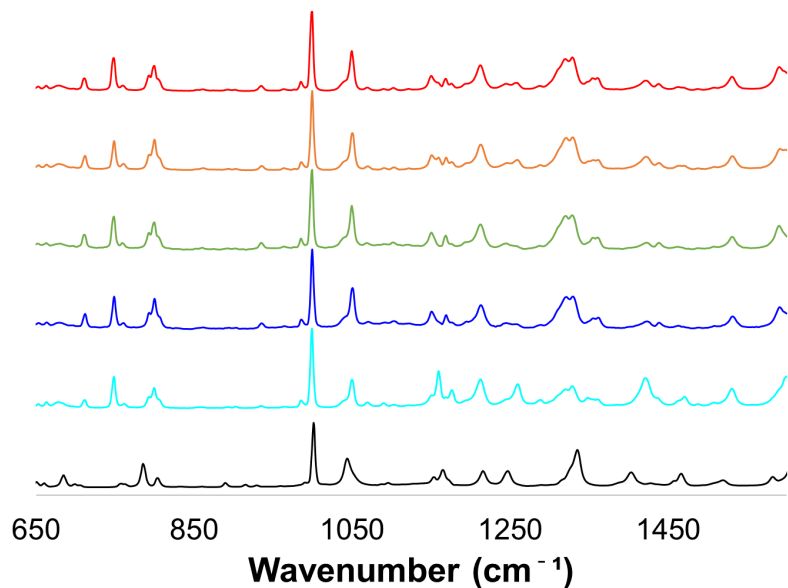


Figure S18. Representative Raman spectra of FFA form III crystals obtained in 1-propanol at a heating rate of 0.3 K/min; $x = 0.1635$ (red), $x = 0.1382$ (orange), $x = 0.1111$ (green), $x = 0.0919$ (blue), FFA form I (black), and FFA form III (cyan). The other molar fractions ($x = 0.0417$, $x = 0.0480$, $x = 0.0608$, $x = 0.0733$) did not recrystallize; therefore, they were not analyzed.

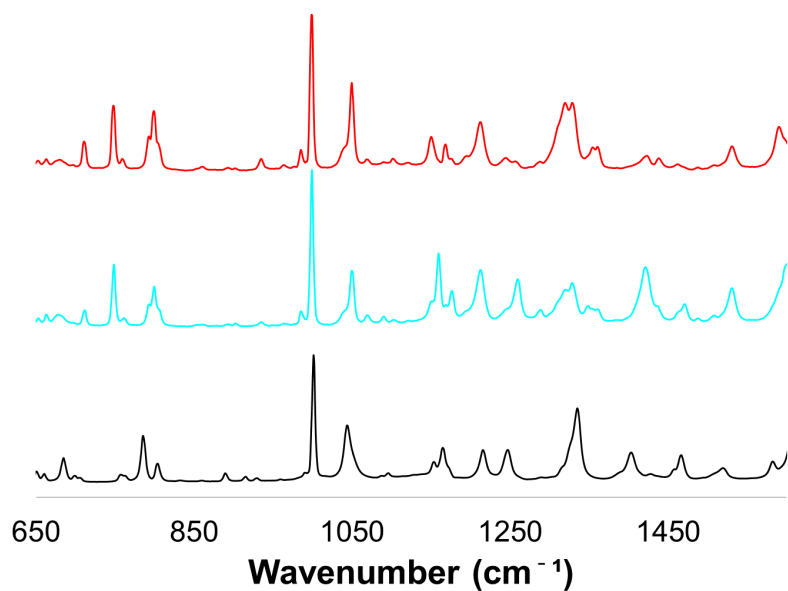


Figure S19. Representative Raman spectra of FFA form III crystals obtained in 1-propanol at a heating rate of 0.1 K/min; $x = 0.0724$ (red), FFA form I (black), and FFA form III (cyan). The other molar fractions ($x = 0.0417$, $x = 0.0476$, $x = 0.0605$, $x = 0.0910$, $x = 0.1112$, $x = 0.1382$, $x = 0.1636$) did not recrystallize; therefore, they were not analyzed.

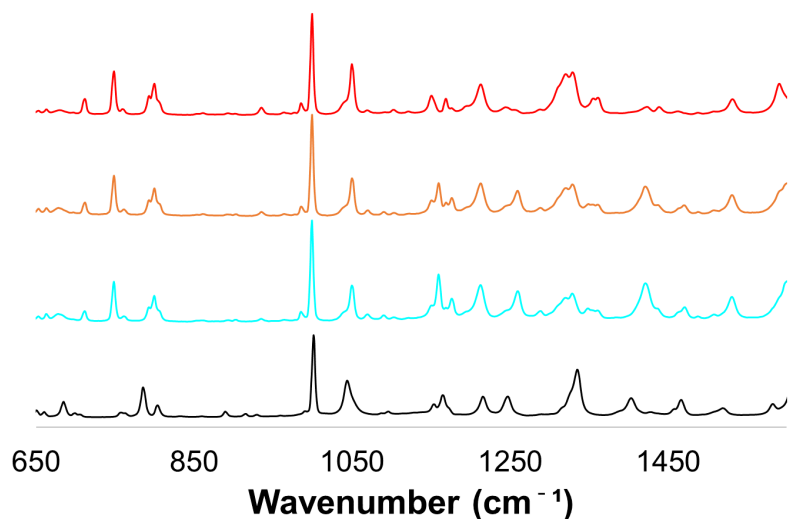


Figure S20. Representative Raman spectra of FFA form I crystals obtained in *n*-butanol at a heating rate of 0.3 K/min; $x_1 = 0.1792$ (red), $x_1 = 0.1363$ (orange), FFA form I (black), and FFA form III (cyan). The other molar fractions ($x_1 = 0.1439$, $x_1 = 0.1518$) did not recrystallize; therefore, they were not analyzed.

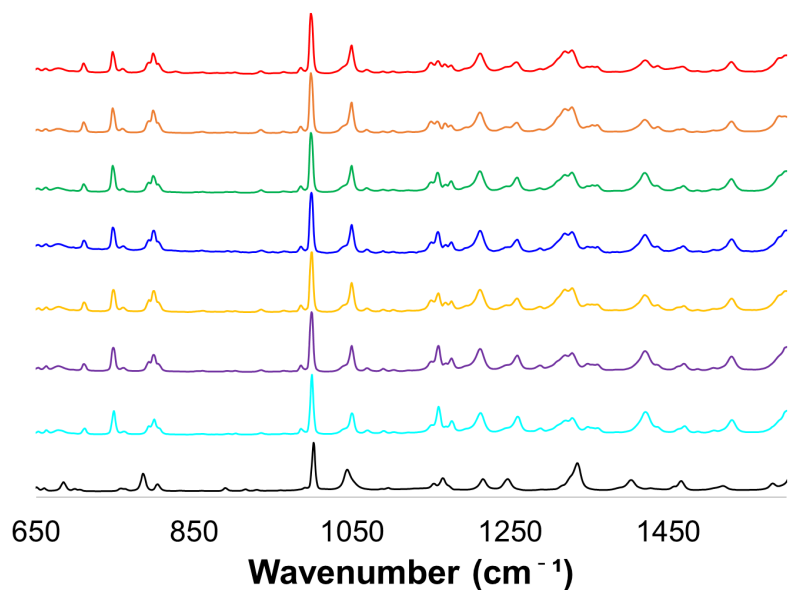


Figure S21. Representative Raman spectra of FFA form III crystals obtained in *n*-butanol at a heating rate of 0.3 K/min; $x_1 = 0.1730$ (red), $x_1 = 0.1514$ (orange), $x_1 = 0.1318$ (green), $x_1 = 0.1141$ (blue), $x_1 = 0.0926$ (yellow), $x_1 = 0.0631$ (purple), FFA form I (black), and FFA form III (cyan). The other molar fractions ($x_1 = 0.0420$, $x_1 = 0.0486$, $x_1 = 0.0672$) did not recrystallize; therefore, they were not analyzed.

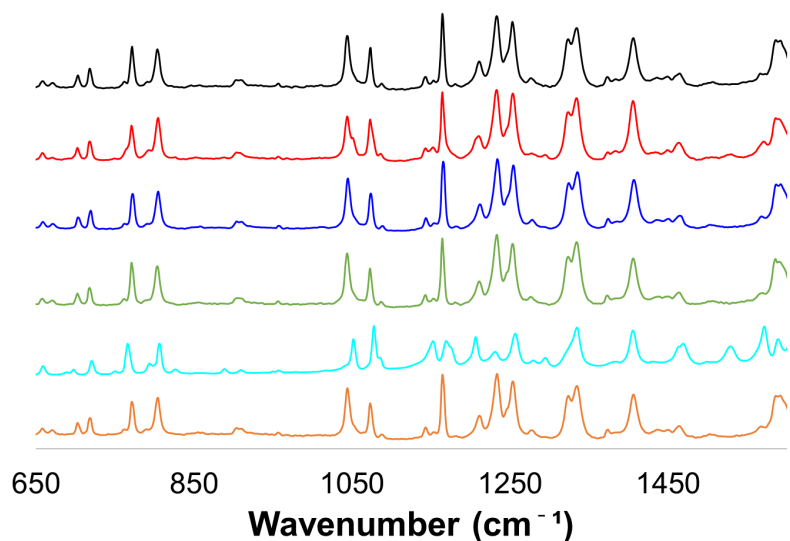


Figure S22. Representative Raman spectra of TA crystals obtained at a heating rate of 0.3 K/min in four pure solvents (top to bottom); methanol (black), ethanol (red), 1-propanol (blue), *n*-butanol (green), and commercial “as received” TA form I (orange) and recrystallized TA form II (cyan).

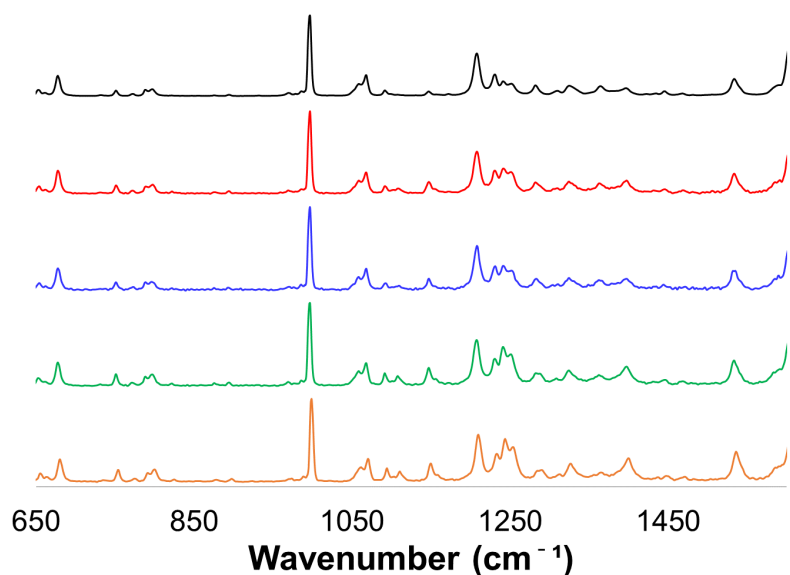


Figure S23. Representative Raman spectra of NA crystals obtained at a heating rate of 0.3 K/min in four pure solvents (top to bottom); methanol (black), ethanol (red), 1-propanol (blue), *n*-butanol (green), and commercial “as received” NA (orange).

7 Powder X-ray Diffraction (PXRD) Analysis

Powder X-ray diffractograms were collected for all polycrystalline samples using a Rigaku XtaLAB SuperNova single micro-focus Cu-K α radiation ($\lambda = 1.5417 \text{ \AA}$) source equipped with a HyPix3000 X-ray detector in transmission mode operating at 50 kV and 1 mA. Powder samples were mounted in MiTeGen

micro loops in the presence of a minimal amount of paratone oil. Powder diffractograms were collected at 300 K over an angular 2θ range between $10 - 50^\circ$ with a step of 0.01° using the Gandolfi move experiment for powders (90 s exposures). Data were analyzed within the *CrystAllisPRO* software (v. 1.171.3920a). The commercial powders of FFA forms I and III, TA forms I and II, and NA were analyzed by PXRD prior to the solubility measurements, and the solid-state confirmed to be the same as that of the starting polymorph.^{6,7,20} All suspensions were measured by PXRD after the experiments were completed. If PXRD diffractograms for specific concentrations (especially lower concentrations) and compound-solvent systems (especially at lower heating rates of 0.1 and 0.05 K/min) are not shown, no crystalline material could be recovered (samples did not recrystallize in the given experimental time). Figures S24-S35 show the PXRD of the recovered material at the end of the heating/cooling cycle(s) for the data points employed in the solubility curves of each of the compounds and polymorphs thereof. We have chosen to include these points in the solubility curve based on the *in situ* and offline solid state characterization. However, we would like to clarify that the recovered crystals at the end of the heating/cooling cycle(s) does not necessarily correspond to that of the starting form employed for each compound and polymorph thereof emphasizing the importance of solid-state monitoring for accurate solubility measurement, particularly if the intend is to average the solubility obtained during different heating/cooling cycles.

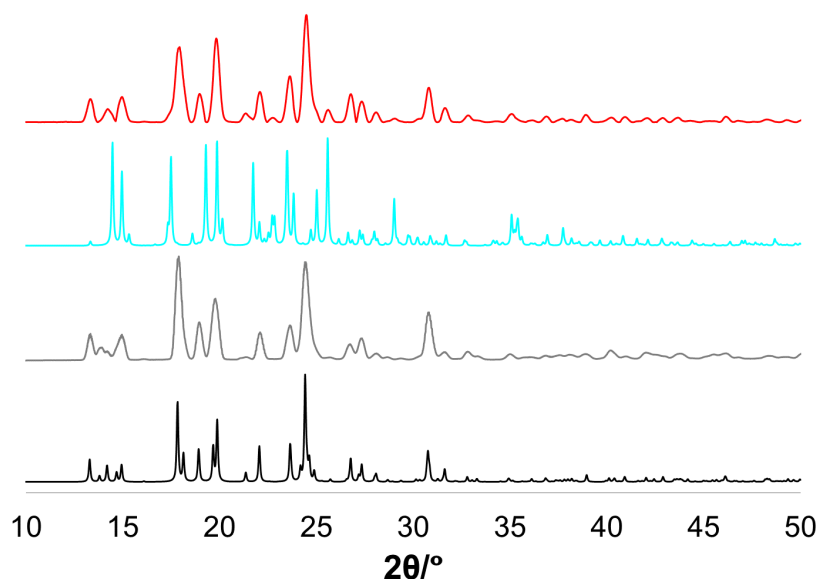


Figure S24. Representative powder X-ray diffractograms of FFA form I crystals obtained in methanol at a heating rate of 0.3 K/min; $x_1 = 0.1263$ (red), compared to the simulated diffractograms of FFA forms I and III (Reference Codes = FPAMCA11²¹ and FPAMCA,⁹ respectively) obtained from the Cambridge Structural Database, CSD (bottom, black and upper, cyan), and to the commercial “as received” FFA (gray). The other molar fractions ($x_1 = 0.0925$, $x_1 = 0.0968$, $x_1 = 0.1036$, $x_1 = 0.1147$) did not recrystallize; therefore, they were not analyzed.

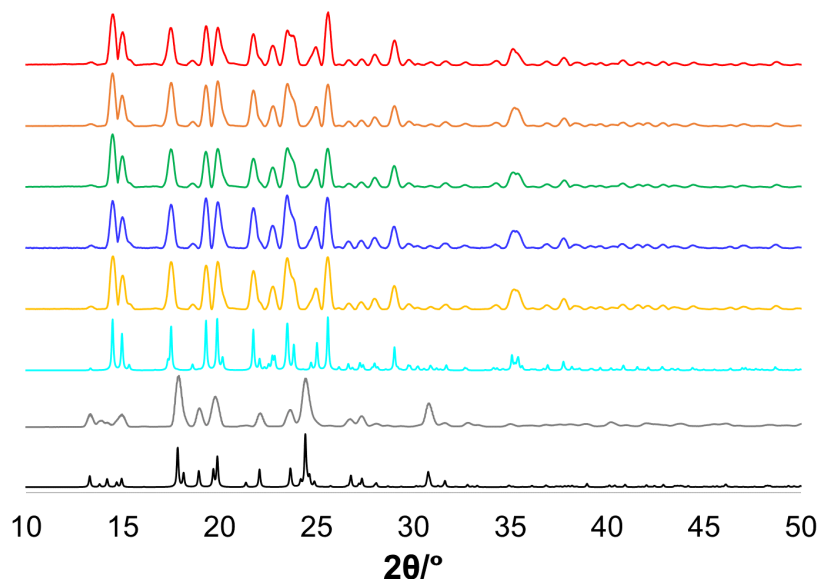


Figure S25. Representative powder X-ray diffractograms of FFA form III crystals obtained in methanol at a heating rate of 0.3 K/min; $x_1 = 0.1248$ (red), $x_1 = 0.1042$ (orange), $x_1 = 0.0907$ (green), $x_1 = 0.0587$ (blue), $x_1 = 0.0443$ (yellow), compared to the simulated diffractograms of FFA forms I and III (Reference Codes = FPAMCA11²¹ and FPAMCA,⁶ respectively) obtained from the Cambridge Structural Database, CSD (bottom, black and upper, cyan), and to the commercial “as received” FFA (gray). The other molar fractions ($x_1 = 0.0264$, $x_1 = 0.0313$, $x_1 = 0.0380$) did not recrystallize; therefore, they were not analyzed.

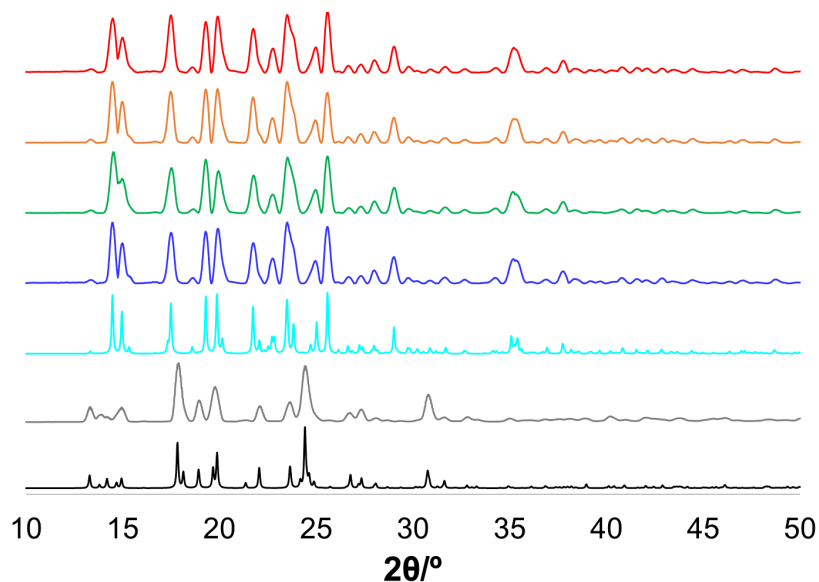


Figure S26. Representative powder X-ray diffractograms of FFA form I crystals obtained in ethanol at a heating rate of 0.3 K/min; $x_1 = 0.1552$ (red), $x_1 = 0.1493$ (orange), $x_1 = 0.1476$ (green), $x_1 = 0.1421$ (blue), compared to the simulated diffractograms of FFA forms I and III (Reference Codes = FPAMCA11²¹ and FPAMCA,⁶ respectively) obtained from the Cambridge Structural Database, CSD (bottom, black and upper, cyan), and to the commercial “as received” FFA (gray). The other molar fractions ($x_1 = 0.1228$, $x_1 = 0.1278$) did not recrystallize; therefore, they were not analyzed.

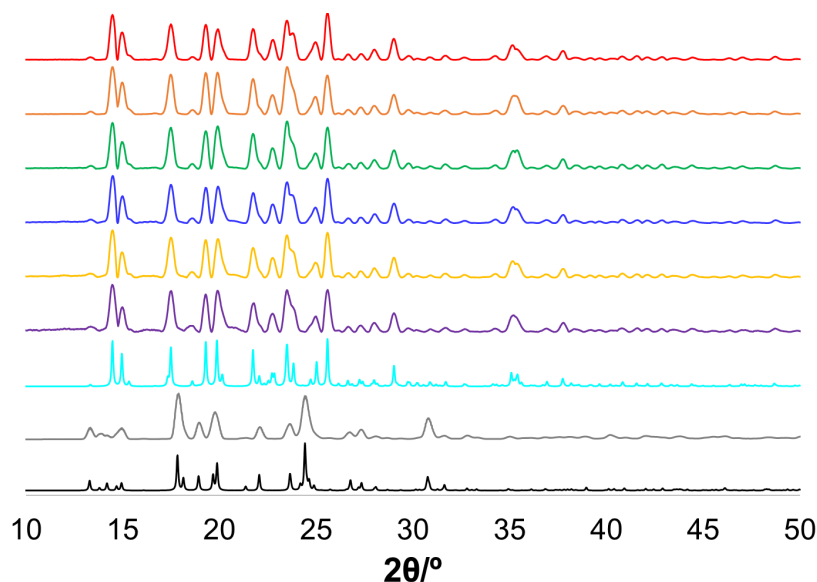


Figure S27. Representative powder X-ray diffractograms of FFA form III crystals obtained in ethanol at a heating rate of 0.3 K/min; $x_1 = 0.1557$ (red), $x_1 = 0.1493$ (orange), $x_1 = 0.1360$ (green), $x_1 = 0.1019$ (blue), $x_1 = 0.0870$ (yellow), $x_1 = 0.0739$ (purple), compared to the simulated diffractograms of FFA forms I and III (Reference Codes = FPAMCA11²¹ and FPAMCA,⁵ respectively) obtained from the Cambridge Structural Database, CSD (bottom, black and upper, cyan), and to the commercial “as received” FFA (gray). The other molar fractions ($x_1 = 0.0352$, $x_1 = 0.0543$, $x_1 = 0.0588$) did not recrystallize; therefore, they were not analyzed.

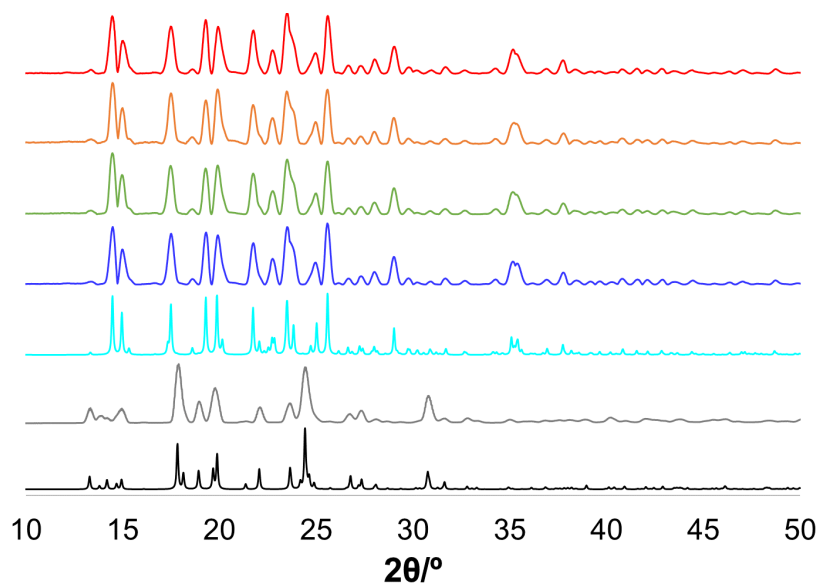


Figure S28. Representative powder X-ray diffractograms of FFA form I crystals obtained in 1-propanol at a heating rate of 0.3 K/min; $x_1 = 0.1616$ (red), $x_1 = 0.1579$ (orange), $x_1 = 0.1477$ (green), $x_1 = 0.1393$ (blue), compared to the simulated diffractograms of FFA forms I and III (Reference Codes = FPAMCA11²¹ and FPAMCA,⁵ respectively) obtained from the Cambridge Structural Database, CSD (bottom, black and upper, cyan), and to the commercial “as received” FFA (gray). The other molar fractions ($x_1 = 0.1284$, $x_1 = 0.1371$) did not recrystallize; therefore, they were not analyzed.

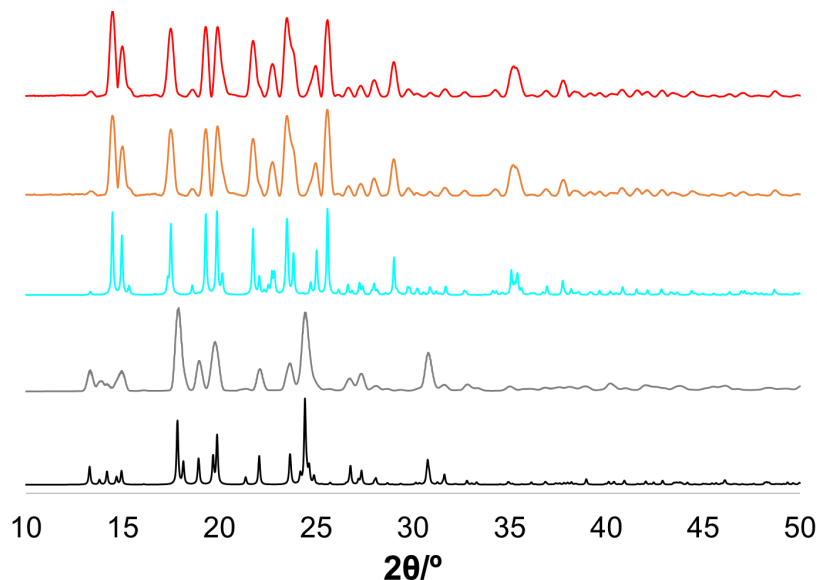


Figure S29. Representative powder X-ray diffractograms of FFA form I crystals obtained in 1-propanol at a heating rate of 0.1 K/min; $x = 0.1473$ (red), $x = 0.1371$ (orange), compared to the simulated diffractograms of FFA forms I and III (Reference Codes = FPAMCA11²¹ and FPAMCA,⁶ respectively) obtained from the Cambridge Structural Database, CSD (bottom, black and upper, cyan), and to the commercial “as received” FFA (gray). The other molar fractions ($x = 0.1284$, $x = 0.1346$) did not recrystallize; therefore, they were not analyzed.

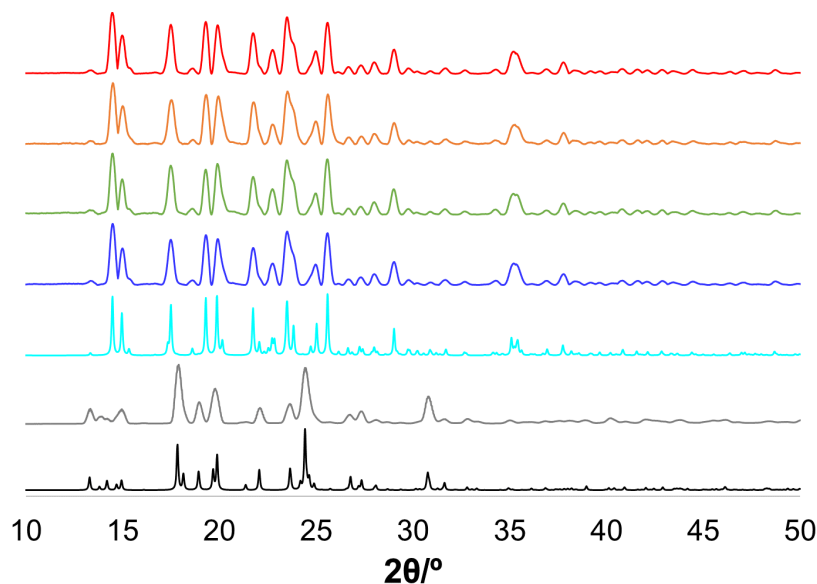


Figure S30. Representative powder X-ray diffractograms of FFA form III crystals obtained in 1-propanol at a heating rate of 0.3 K/min; $x_1 = 0.1635$ (red), $x_1 = 0.1382$ (orange), $x_1 = 0.1111$ (green), $x_1 = 0.0919$ (blue), compared to the simulated diffractograms of FFA forms I and III (Reference Codes = FPAMCA11²¹ and FPAMCA,⁶ respectively) obtained from the Cambridge Structural Database, CSD (bottom, black and upper, cyan), and to the commercial “as received” FFA (gray). The other molar fractions ($x_1 = 0.0417$, $x_1 = 0.0480$, $x_1 = 0.0608$, $x_1 = 0.0733$) did not recrystallize; therefore, they were not analyzed.

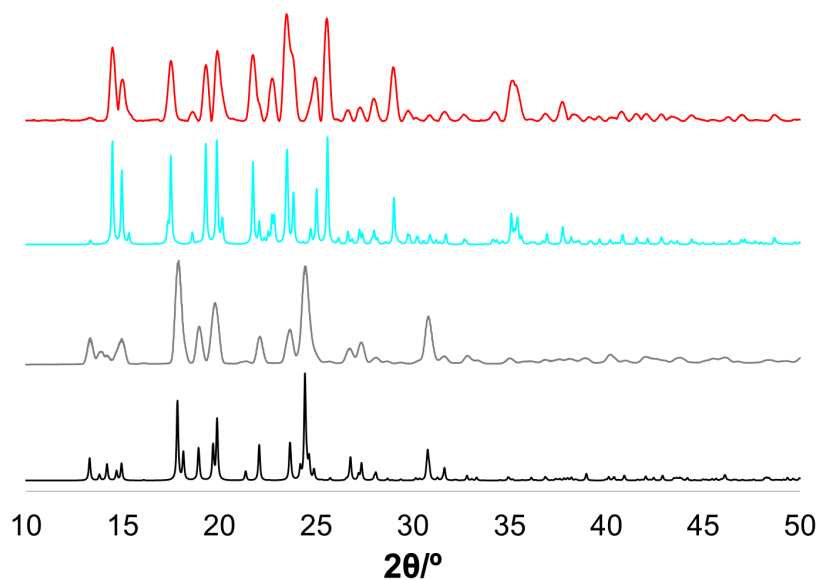


Figure S31. Representative powder X-ray diffractograms of FFA form III crystals obtained in 1-propanol at a heating rate of 0.1 K/min; $x = 0.0724$ (red), compared to the simulated diffractograms of FFA forms I and III (Reference Codes = FPAMCA11²¹ and FPAMCA,⁶ respectively) obtained from the Cambridge Structural Database, CSD (bottom, black and upper, cyan), and to the commercial “as received” FFA (gray). The other molar fractions ($x = 0.0417$, $x = 0.0476$, $x = 0.0605$, $x = 0.0910$, $x = 0.1112$, $x = 0.1382$, $x = 0.1636$) did not recrystallize; therefore, they were not analyzed.

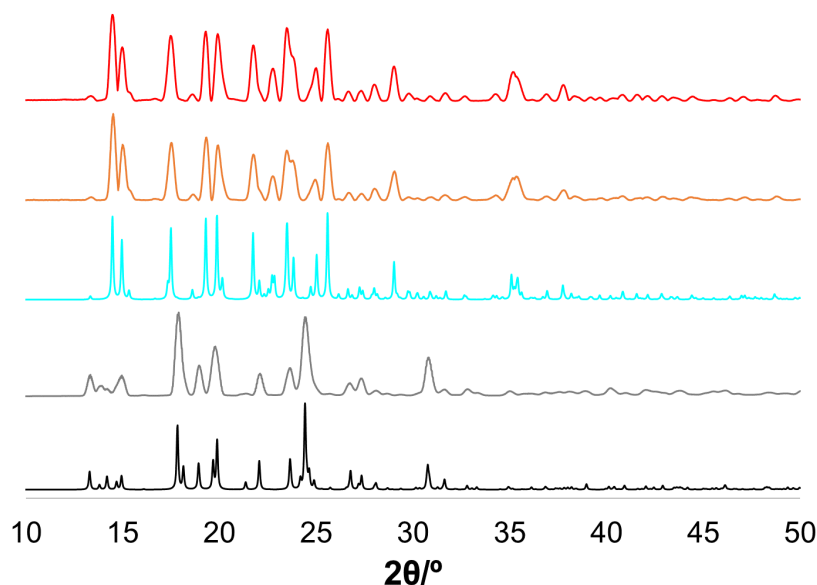


Figure S32. Representative powder X-ray diffractograms of FFA form I crystals obtained in n-butanol at a heating rate of 0.3 K/min; $x_1 = 0.1792$ (red), $x_1 = 0.1363$ (orange), compared to the simulated diffractograms of FFA forms I and III (Reference Codes = FPAMCA11²¹ and FPAMCA,⁶ respectively) obtained from the Cambridge Structural Database, CSD (bottom, black and upper, cyan), and to the commercial “as received” FFA (gray). The other molar fractions ($x_1 = 0.1439$, $x_1 = 0.1518$) did not recrystallize; therefore, they were not analyzed.

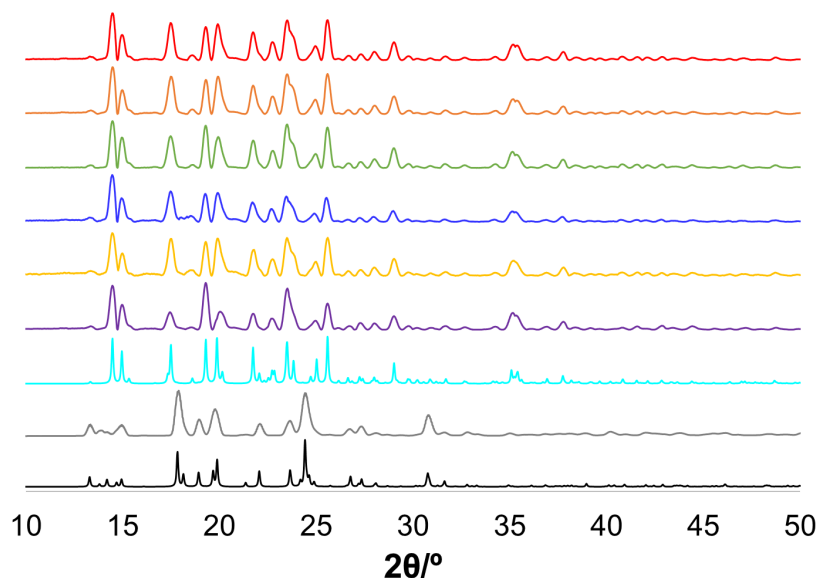


Figure S33. Representative powder X-ray diffractograms of FFA form III crystals obtained in n-butanol at a heating rate of 0.3 K/min; $x_1 = 0.1730$ (red), $x_1 = 0.1514$ (orange), $x_1 = 0.1318$ (green), $x_1 = 0.1141$ (blue), $x_1 = 0.0926$ (yellow), $x_1 = 0.0631$ (purple), compared to the simulated diffractograms of FFA forms I and III (Reference Codes = FPAMCA11²¹ and FPAMCA⁶, respectively) obtained from the Cambridge Structural Database, CSD (bottom, black and upper, cyan), and to the commercial “as received” FFA (gray). The other molar fractions ($x_1 = 0.0420$, $x_1 = 0.0486$, $x_1 = 0.0672$) did not recrystallize; therefore, they were not analyzed.

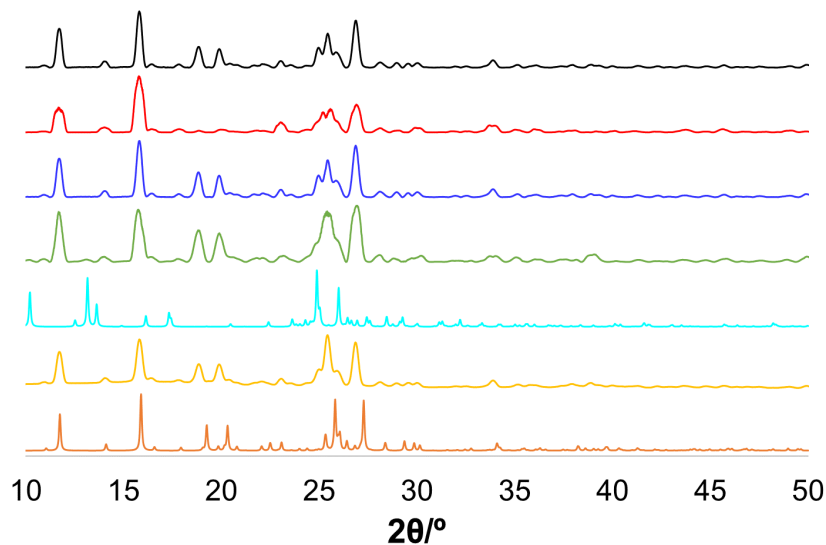


Figure S34. Representative powder X-ray diffractograms of TA crystals obtained at a heating rate of 0.3 K/min in four pure solvents (top to bottom); methanol (black), ethanol (red), 1-propanol (blue), n-butanol (green), compared to the simulated diffractograms of TA forms I and II (Reference Codes = KAXXAI01 and KAXXAI²³, respectively) obtained from the Cambridge Structural Database, CSD (bottom, orange and upper, cyan), and to the commercial “as received” TA (yellow).

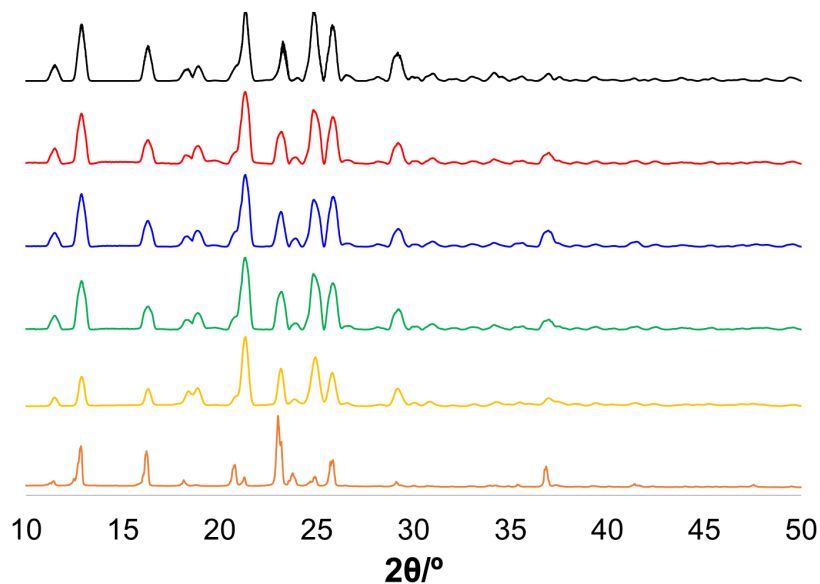


Figure S35. Representative powder X-ray diffractograms of NA crystals obtained at a heating rate of 0.3 K/min in four pure solvents (top to bottom); methanol (black), ethanol (red), 1-propanol (blue), *n*-butanol (green), compared to the simulated diffractograms of NA form I (Reference Code = NIFLUM10³⁰) obtained from the Cambridge Structural Database, CSD (bottom, orange), and to the commercial “as received” NA (yellow).

8 *In situ* Raman Spectroscopy

In situ Raman spectra were recorded over the range of 200 – 1900 cm⁻¹ employing a RamanRxn2TM Multi-channel Raman Analyzer (Kaiser Optical Systems) equipped with an immersion probe (6.35 mm) and a 785 nm laser. For each compound the acquisition conditions were optimized so that spectra were captured in 1 min intervals with 10 accumulations and an exposure time of 3 s for FFA form III, TA form I, and TA form II, 1 s for FFA I, and 0.5 s for NA per measurement with automatic cosmic ray filter and intensity correction using iC Raman software (v. 4.1.917). The probe was immersed from the top into a Crystalline multiple reactor system (Technobis Crystallization Systems) using sealed glass vials (Fisher Scientific, internal volume of 8 mL) with a 2 mL starting volume of the suspension agitated using a rare earth magnetic stir bar at 700 rpm to enable parallel visual measurement capabilities using the onboard camera system. All preparative and experimental procedures were applied as described for the Crystall16 in the Solubility Measurement section. Figures S36-S39 show the *in situ* Raman analysis coupled with solubility measurement for FFA form III, TA forms I and II, and NA from 278.15 to 333.15 K in 1-propanol at a heating rate of 0.3 K/min.

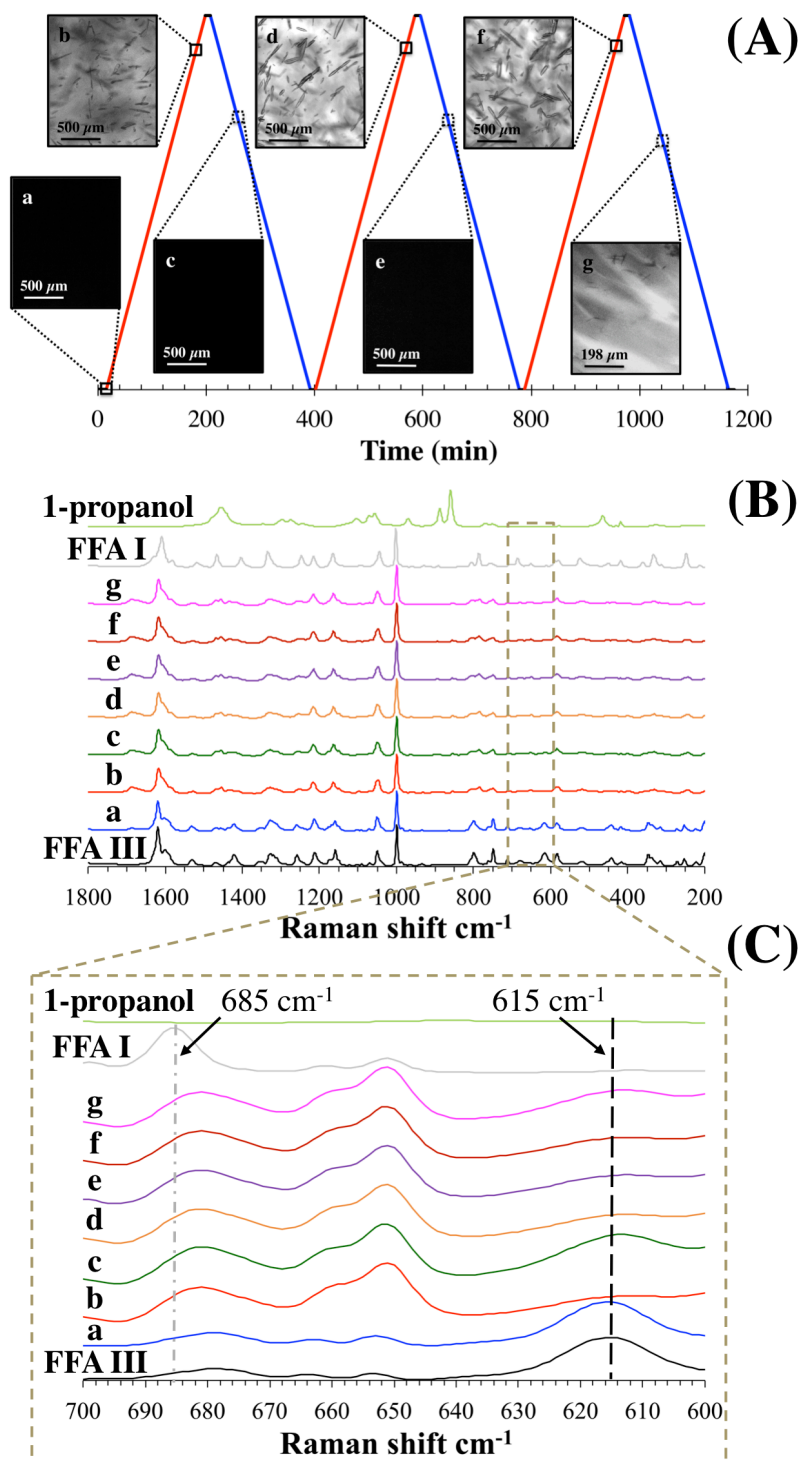


Figure S36. Solubility experiments of FFA form III in 1-propanol employing *in situ* Raman spectroscopy in Crystalline system (A) micrographs recorded in respective temperature profile from 278.15 to 333.15 K at a heating rate of 0.3 K/min, (B) *in situ* Raman spectra, and (C) cut out of specific Raman shift: (a) prior to 1st heating cycle, (b) close to solubility point in 1st heating cycle, (c) nucleation in 1st cooling cycle, (d) close to solubility point in 2nd heating cycle, (e) nucleation in 2nd cooling cycle, (f) close to solubility point in 3rd heating cycle, and (g) nucleation in 3rd cooling cycle.

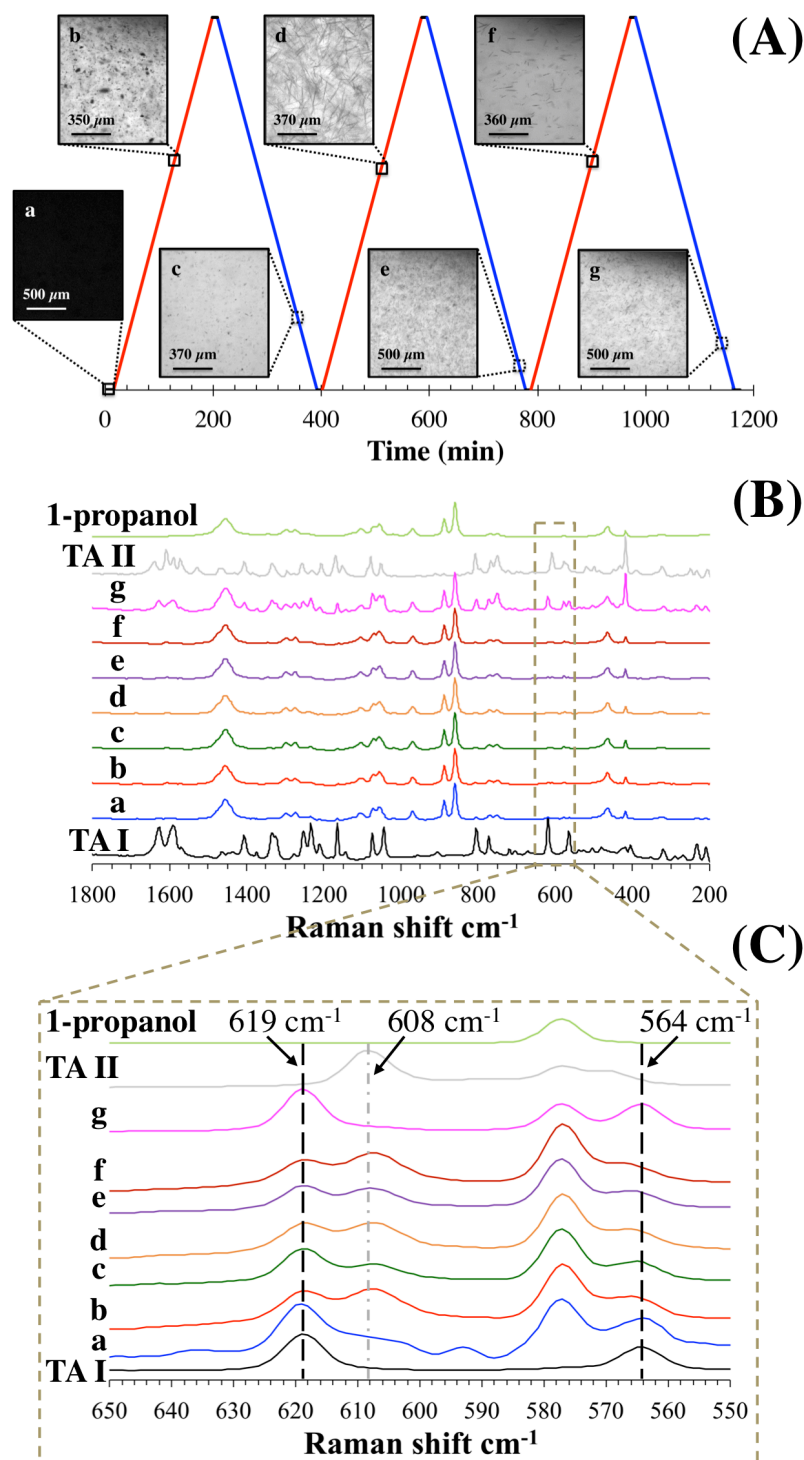


Figure S37. Solubility experiments of TA form I in 1-propanol employing *in situ* Raman spectroscopy in Crystalline system (A) micrographs recorded in respective temperature profile from 278.15 to 333.15 K at a heating rate of 0.3 K/min, (B) *in situ* Raman spectra, and (C) cut out of specific Raman shift: (a) prior to 1st heating cycle, (b) close to solubility point in 1st heating cycle, (c) nucleation in 1st cooling cycle, (d) close to solubility point in 2nd heating cycle, (e) nucleation in 2nd cooling cycle, (f) close to solubility point in 3rd heating cycle, and (g) nucleation in 3rd cooling cycle.

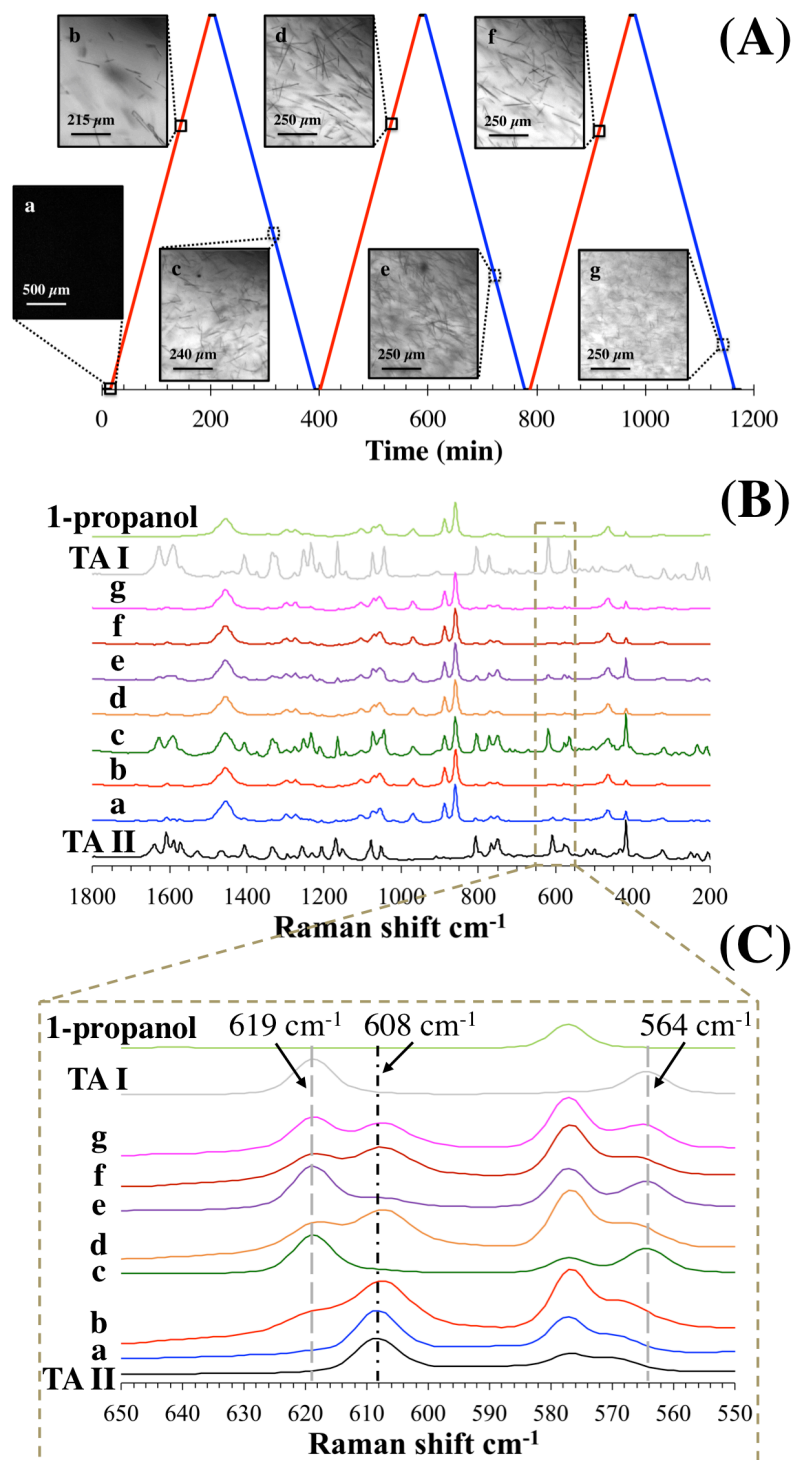


Figure S38. Solubility experiments of TA form II in 1-propanol employing *in situ* Raman spectroscopy in Crystalline system (A) micrographs recorded in respective temperature profile from 278.15 to 333.15 K at a heating rate of 0.3 K/min, (B) *in situ* Raman spectra, and (C) cut out of specific Raman shift: (a) prior to 1st heating cycle, (b) close to solubility point in 1st heating cycle, (c) nucleation in 1st cooling cycle, (d) close to solubility point in 2nd heating cycle, (e) nucleation in 2nd cooling cycle, (f) close to solubility point in 3rd heating cycle, and (g) nucleation in 3rd cooling cycle.

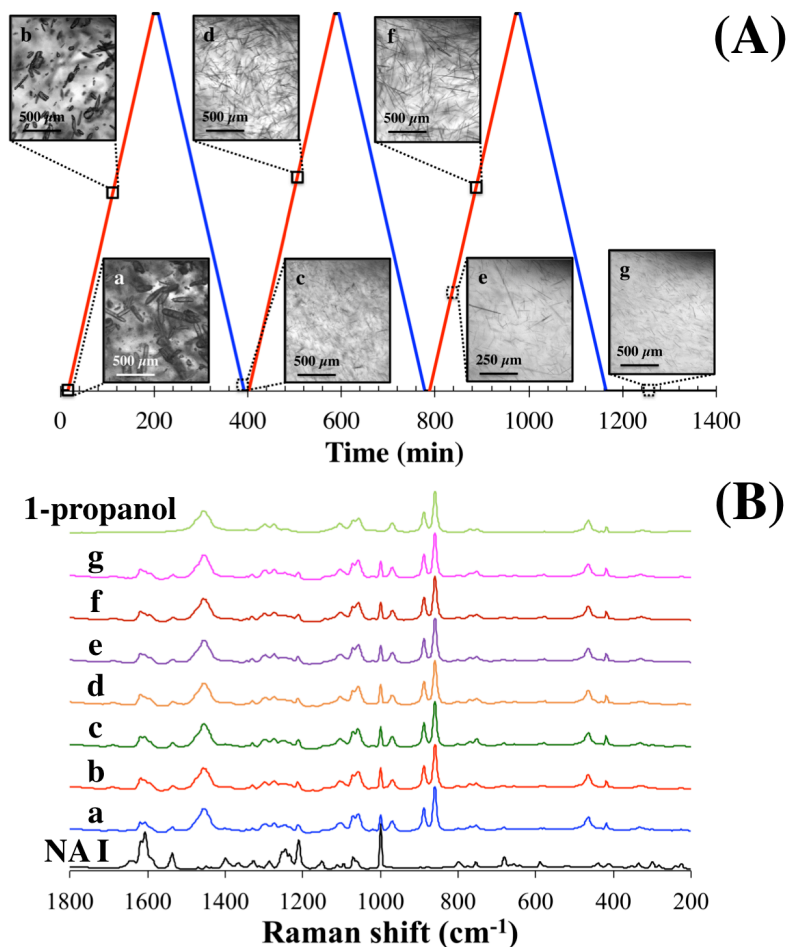


Figure S39. Solubility experiments of NA in 1-propanol employing *in situ* Raman spectroscopy in Crystalline system (A) micrographs recorded in respective temperature profile from 278.15 to 333.15 K at a heating rate of 0.3 K/min and (B) *in situ* Raman spectra: (a) prior to 1st heating cycle, (b) close to solubility point in 1st heating cycle, (c) nucleation in 1st cooling cycle, (d) close to solubility point in 2nd heating cycle, (e) nucleation in 2nd cooling cycle, (f) close to solubility point in 3rd heating cycle, and (g) nucleation in 3rd cooling cycle.

9 References

- (1) Purdief. Guidance for Industry Q3C. *U.S. Dep. Heal. Hum. Serv. Food, Food Drug Adm.* **2012**, 9765, 301–827.
- (2) Gilpin, R. K.; Zhou, W. Infrared Studies of the Polymorphic States of the Fenamates. *J. Pharm. Biomed. Anal.* **2005**, *37*, 509–515.
- (3) Andersen, K. V.; Larsen, S.; Alhede, B.; Gelting, N.; Buchardt, O. Characterization of Two Polymorphic Forms of Tolfenamic Acid, N-(2-Methyl-3-Chlorophenyl)Anthranilic Acid: Their Crystal Structures and Relative Stabilities. *J. Chem. Soc. Perkin Trans. II* **1989**, 1443–1447.

- (4) Lee, E.; Byrn, S. R.; Pinal, R. The Solution Properties of Mefenamic Acid and a Closely Related Analogue Are Indistinguishable in Polar Solvents but Significantly Different in Nonpolar Environments. *J. Pharm. Sci.* **2012**, *101*, 4529–4539.
- (5) Domańska, U.; Pobudkowska, A.; Pelczarska, A. Solubility of Sparingly Soluble Drug Derivatives of Anthranilic Acid. *J. Phys. Chem. B* **2011**, *115*, 2547–2554.
- (6) López-Mejías, V.; Kampf, J. W.; Matzger, A. J. Nonamorphism in Flufenamic Acid and a New Record for a Polymorphic Compound with Solved Structures. *J. Am. Chem. Soc.* **2012**, *134*, 9872–9875.
- (7) López-Mejías, V.; Kampf, J. W.; Matzger, A. J. Polymer-Induced Heteronucleation of Tolfenamic Acid: Structural Investigation of a Pentamorph. *J. Am. Chem. Soc.* **2009**, *131*, 4554–4555.
- (8) Chen, H.; Su, C.; Liu, J.; Sheu, M. The Journal of Supercritical Fluids Solid-State Property Modification and Dissolution Rate Enhancement of Tolfenamic Acid by Supercritical Antisolvent Process. *J. Supercrit. Fluids* **2015**, *101*, 17–23.
- (9) Nyvlt; Nývlt, J. Kinetics of Nucleation in Solutions. *J. Cryst. Growth* **1968**, *3*, 377–383.
- (10) Pascual, G. K.; Donnellan, P.; Glennon, B.; Kamaraju, V. K.; Jones, R. C. Experimental and Modeling Studies on the Solubility of 2-Chloro-N-(4-Methylphenyl)Propanamide (S1) in Binary Ethyl Acetate + Hexane, Toluene + Hexane, Acetone + Hexane, and Butanone + Hexane Solvent Mixtures Using Polythermal Method. *J. Chem. Eng. Data* **2017**, *62*, 3193–3205.
- (11) Wei, T.; Wang, C.; Du, S.; Wu, S.; Li, J.; Gong, J. Measurement and Correlation of the Solubility of Penicillin V Potassium in Ethanol + Water and 1-Butyl Alcohol + Water Systems. *J. Chem. Eng. Data* **2015**, *60*, 112–117.
- (12) Reus, M. a.; van der Heijden, A. E. D. M.; ter Horst, J. H. Solubility Determination from Clear Points upon Solvent Addition. *Org. Process Res. Dev.* **2015**, *19*, 1004–1011.
- (13) Vellema, J.; Hunfeld, N. G. M.; Akker, H. E. A. Van Den; Horst, J. H. Avoiding Crystallization of Lorazepam during Infusion. *Eur. J. Pharm. Sci.* **2011**, *44*, 621–626.
- (14) Kaemmerer, H.; Jones, M. J.; Lorenz, H.; Seidel-Morgenstern, A. Selective Crystallisation of a Chiral Compound-Forming System-Solvent Screening, SLE Determination and Process Design. *Fluid Phase Equilib.* **2010**, *296*, 192–205.
- (15) Monbaliu, J.-C. M.; Stelzer, T.; Revalor, E.; Weeranoppanant, N.; Jensen, K. F.; Myerson, A. S. Compact and Integrated Approach for Advanced End-to-End Production, Purification, and Aqueous Formulation of Lidocaine Hydrochloride. *Org. Process Res. Dev.* **2016**, *20*, 1347–1353.
- (16) Zorrilla-Veloz, R. I.; Stelzer, T.; López-Mejías, V. Measurement and Correlation of the Solubility of 5-Fluorouracil in Pure and Binary Solvents. *J. Chem. Eng. Data* **2018**, *63*, 3809–3817.

- (17) Hu, Y.; Liang, J. K.; Myerson, A. S.; Taylor, L. S. Crystallization Monitoring by Raman Spectroscopy: Simultaneous Measurement of Desupersaturation Profile and Polymorphic Form in Flufenamic Acid Systems. *Ind. Eng. Chem. Res.* **2005**, *44*, 1233–1240.
- (18) Guo, Y.; Yin, Q.; Hao, H.; Zhang, M.; Bao, Y.; Hou, B.; Chen, W.; Zhang, H.; Cong, W. Measurement and Correlation of Solubility and Dissolution Thermodynamic Properties of Furan-2-Carboxylic Acid in Pure and Binary Solvents. *J. Chem. Eng. Data* **2014**, *59*, 1326–1333.
- (19) George De la Rosa, M. V.; Santiago, R.; Malavé Romero, J.; Duconge, J.; Monbaliu, J.-C.; López-Mejías, V.; Stelzer, T. Solubility Determination and Correlation of Warfarin Sodium 2-Propanol Solvate in Pure, Binary, and Ternary Solvent Mixtures. *J. Chem. Eng. Data* **2019**, *64*, 1399–1413.
- (20) Vijayan, H. M. Krishna, M. M. 2-[3-(Trifluoromethyl)Phenyl]Amino}- 3-Pyridinecarboxylic Acid (Niflumic Acid). *Acta Crystallogr.* **1979**, *B35*, 262–203.
- (21) Krishna Murthy, H. M.; Bhat, T. N.; Vuayan, M. Structure of a New Crystal Form of 2-[3-(Trifluoromethyl)Phenyl]Amino}benzoic Acid (Flufenamic Acid). *Acta Crystallogr.* **1982**, *B38*, 315–317.